Proceedings of the 11th World Congress on New Technologies (NewTech'25)
Paris, France - August, 2025
Paper No. ICERT 142
DOI: 10.11159/icert25.142

Experimental Measurement and Machine Learning Modelling for the Density of Hybrid Nanofluids

Emmanuel O. Atofarati [1], Christopher Enweremadu [2]
[1] Department of Mechanical, Bioresources and Biomedical Engineering, University of South Africa
Florida Campus, Private Bag 392, Johannesburg, 2449, South Africa
atofae@unisa.ac.za; enwercc@unisa.ac.za
[2] Department of Mechanical, Bioresources and Biomedical Engineering, University of South Africa
Florida Campus, Private Bag 392, Johannesburg, 2449, South Africa

Abstract - Accurate prediction of nanofluid density is crucial for enhancing heat transfer efficiency in energy systems, such as solar thermal and geo-thermal systems. However, existing nanofluid models often fail to capture the interactions of hybrid nanoparticles in hybrid base fluid. This study experimentally investigates the density behavior of single, bi-hybrid, and ternary-hybrid nanofluids and applies machine learning models to improve predictive accuracy. The nanofluids composed of Al_2O_3, Fe_3O_4, and MWCNT nanoparticles synthesized in deionized water (DIW), ethylene glycol (EG), and DIW-EG mixtures. Density measurements were conducted at temperature ($10°C < T < 50°C$) and nanoparticle volume fractions (0 vol% $< \phi <$ 6.0 vol%) using a simple glass pycnometer. Linear Regression was employed for density prediction, while Random Forest, Support Vector Machine (SVM), and Gradient Boosting were selected for classification due to their robustness to non-linear relationships and high interpretability. These models were assessed using accuracy and F1-score, with Gradient Boosting and Random Forest achieving the best performance (>94% accuracy). Results showed that single nanofluids (Al_2O_3-based) exhibited density variations influenced by temperature and volume fraction. Bi-hybrid nanofluids (Al_2O_3-MWCNT) had higher densities due to MWCNT reinforcement. Ternary-hybrid nanofluids (Al_2O_3-MWCNT-Fe_3O_4) displayed the highest densities, particularly in EG-based mixtures, attributed to high density Fe_3O_4 nanoparticle and that of EG. Feature importance analysis confirmed volume fraction and base fluid composition as dominant factors influencing the density of the nanofluids. By integrating experimental data into machine learning algorithms, this study improves nanofluid density prediction, offering insights for optimizing thermal management in energy and industrial systems.

***Keywords*:** Density; Hybrid Nanofluid; Thermophysical Properties; Correlations; Machine learning; Feature importance

1. Introduction

Nanofluids are suspensions of nanoparticles within base fluids and have emerged as a promising class of materials due to their superior thermo-physical properties compared to conventional fluids [1]. Their enhanced properties, which include increased thermal conductivity, specific heat capacity, and density, position nanofluids as ideal heat transfer medium for applications in engineering systems such as cooling devices [2], heat exchangers [3], [4], and renewable energy technologies [5], [6]. Among these properties, effective density plays a pivotal role in determining the performance and efficiency of nanofluid-based thermal systems.

The density of a nanofluid is a critical parameter that interacts with other thermophysical properties, particularly thermal conductivity, viscosity, and specific heat capacity, to determine its overall heat transfer performance [7]–[9]. In thermal energy systems, density directly influences fluid motion, affecting buoyancy-driven convection, thermal stratification, and pumping power requirements [10]–[12]. A higher-density nanofluid can enhance thermal storage capacity and promote better mixing, leading to improved convective heat transfer. However, increased density often correlates with higher viscosity, which can elevate pumping power demands and impact flow stability. While thermal conductivity is often the primary focus in nanofluid research, its effectiveness is significantly influenced by density-driven fluid motion [13]–[15].

Additionally, density of a nanofluid plays a key role in nanoparticle stability and sedimentation, which are factors that determine the long-term usability of nanofluids [16]–[18]. Given the interdependence of these properties, selecting an optimal nanoparticle composition and base fluid combination is essential for balancing thermal efficiency with practical system constraints [19], [20]. Despite its significance, density has been relatively underexplored compared to thermal conductivity and viscosity, particularly in hybrid nanofluids where multiple nanoparticle or base fluid interactions further complicate

thermophysical behavior. This study focuses on density as a fundamental property governing nanofluid performance, aiming to enhance its predictive modeling using experimental data and machine learning techniques

The classical mixing rule/model is a widely used approach in nanofluid research, which assumes a linear combination of the densities of nanoparticles and base fluid weighted by their volume fractions as proposed by Nielsen [21]. The mixing rule was first reportedly used in the work of Pak and Cho [22]. While convenient to use, this model often fails to accurately account for non-ideal behaviors such as nanoparticle clustering, void formation, and nanolayer effects at higher concentrations. Also, it doesn't account for the influence of temperature on the density of the nanofluid. Several modified forms of this model have been provided in literature as summarized on **Table 1**.

While earlier studies such as Sharifpur et al. [23] and Selvakumar et al. [24] presented theoretically modified mixing (Pak and Cho) model for density of nanofluids, which is only a function of the nanoparticle volume fraction; recent studies utilize statical and artificial intelligent tools to model fitted correlation for the density of respective nanofluids as a function of volume fraction and temperature. Sharifpur et al. [23] investigated the density of nanofluids experimentally, considering SiO_2-water, MgO-glycerol, CuO-glycerol, and SiO_2-ethylene glycol/water mixtures for nanoparticle volume fractions of 1%–6% and temperatures ranging from 10°C to 40°C. The study demonstrated that the widely used mixing model for density overestimates experimental values, particularly at higher nanoparticle concentrations. This discrepancy was attributed to the influence of nanolayer thickness (t_v), an interfacial layer with density between the base fluid and void density. A new density model incorporating the nanolayer's equivalent void thickness was developed, showing strong agreement with experimental data and outperforming the mixing model, especially for volume fractions above 1%. The study also highlighted that void thickness in the nanolayer is more sensitive to nanoparticle size than to base fluid or nanoparticle material.

Similarly, Selvakumar et al. [24] proposed a comprehensive model to predict the effective density of nanofluids, incorporating the effects of nanoparticle clustering and interfacial layer formation. Using Particle Size Distribution (PSD) analysis, the study explicitly calculated the densities of primary nanoparticles and their clusters, considering the interfacial layer with a thickness of ~2 nm and a density ~25% higher than the base fluid. The model integrates these factors into a modified mixture rule to account for increased effective volume fraction due to the interfacial layer. Validation against experimental data revealed that the new model consistently outperformed the traditional mixture rule, with percentage deviations as low as 0.12%, compared to up to 25.19% in the mixture rule, highlighting its superior accuracy for nanofluids in practical heat transfer applications.

Montazer et al. [25] proposed a new density correlation for carbon-based nanofluids using Response Surface Methodology (RSM). Experiments on MWCNT–COOH and F-GNP nanofluids, conducted at mass concentrations up to 0.1% and temperatures between 20–40 °C, showed density increases with mass concentration and decreases with temperature. The RSM quadratic model accurately predicted densities, with maximum deviations of 0.012% for MWCNT–COOH and 0.009% for F-GNP nanofluids. Notably, MWCNT–COOH nanofluids showed a 0.15% density increase at 0.1% concentration, while F-GNP nanofluids exhibited a 0.056% rise compared to base fluids. These results highlight the model's precision and its applicability in optimizing nanofluid-based thermal. Also, Yadav et al. [26] conducted an experimental and regression analysis to study density variations in Al_2O_3/EG, CuO/EG, and CeO_2/EG nanofluids across concentrations (0.2–1.5 vol%) and temperatures (20–80°C). The study revealed a linear relationship between density, concentration, and temperature. High-accuracy plane equations were developed for each nanofluid, achieving correlation coefficients (R^2) near 0.999 for Al_2O_3 and CeO_2 nanofluids, with slightly lower accuracy for CuO/EG due to surfactant effects. These equations enable direct density predictions without requiring base fluid or nanoparticle density data, simplifying density estimation for various nanofluids in thermal and tribological applications

Akilu et al. [27] characterized and modeled the density, thermal conductivity, and viscosity of TiN nanofluids (NFs) with water-ethylene glycol (W/EG) base mixtures at 60:40 and 40:60 ratios using Microsoft Excel with the aid of Levenberg–Marquardt algorithm. Experiments were conducted for volume fractions of 0.25–1.0% and temperatures between 20°C to 40°C. Results showed that density and viscosity decrease with temperature, while thermal conductivity increases with nanoparticle concentration. The W/EG 60:40 mixture achieved a thermal conductivity enhancement of up to 22.5%, whereas the 40:60 mixture exhibited a viscosity increase of 34.3%. Empirical correlations for these properties, accounting

for temperature and concentration, predicted results with deviations within ±15%, offering practical utility in thermal engineering applications.

Artificial Intelligence algorithms, such as Machine Learning and Deep Learning have demonstrated significant potential in capturing complex relationships among nanofluid properties. Shoghl et al. [28] utilized a multilayer perceptron neural network (MLPNN) in MATLAB to generate nonlinear mathematical models which predicts the viscosity and density of Al_2O_3/DW, MWCNT/DW, and GNP/DW nanofluids. Experimental measurements were conducted for volume concentrations of 0.1–1% and temperatures of 30–80°C. Results showed viscosity and density increased with concentration and decreased with temperature, with maximum increases of 41.59% and 5.06% for Al_2O_3/DW. The MLPNN model, optimized at 12 perceptron using the Levenberg-Marquardt algorithm, achieved $R^2 > 0.998$, outperforming the mathematical model ($R^2 > 0.9723$) with minimal errors (< 0.2% for density and < 1% for viscosity). Similar Machine/Deep learning techniques have been utilized in the works of Said et al. [29], [30] and Deymi et al. [31]; although no mathematical expressions for density were provided in these studies. These advancements highlight the value of integrating experimental measurements with artificial intelligence to enhance prediction accuracy and model reliability.

Meanwhile, Chavan and Pise [11] experimentally demonstrates how nanoparticle concentration and temperature influence the effective viscosity and density of nanofluids, revealing that viscosity increases with concentration and decreases with temperature, while density increases with concentration and remains largely unaffected by temperature. Similar outcome are reported in other works by Vajjha et al. [32], Shoghl et al. [28], Jamei et al. [33], and Yousefi and Amoozandeh [34].

Hybrid nanofluids, which combine two or more types of nanoparticles within a single base fluid, offer enhanced thermo-physical properties due to synergistic effects [9], [35]. Hybrid nanofluid have been used in several studies involving internal forced convection [36], [37], external forced convection [10], [38], natural convection [39], [40] and mixed convection [41], [42] and they out performance single nanofluid both in stability and thermal conductivity. However, the complexity introduced by interactions between different nanoparticles and the base fluid necessitates advanced modeling techniques [43]. This complexity underscores the need for comprehensive experimental and statistical investigations.

Table 1: Summary of some Density Models in Literature

Authors	**Nanofluids**	**Study**	**Effective Density Models**
Nielsen (1978) [21]	Classical Mixing rule for two-phase mixture	Theoretical	$\rho_{nf} = \rho_{bf}(1-\varphi) + \varphi\rho_p$
Sharifpur et al. (2016) [23]	SiO_2/H_2O, MgO/Gly, CuO/Gly, SiO_2/EG/H_2O ($1<\varphi<6$ vol%)	Experimental & Theoretical	$\rho_{nf} = \frac{\rho_{bf}(1-\varphi) + \varphi\rho_p}{(1-\varphi) + \varphi(r_p - t_v)^3/r_p^3}$
Selvakumar and Wu (2019) [24]	Al_2O_3/H_2O, /PoE, MWCNT/oil, ZnO/PoE ($0.001<\varphi<0.150$ wt%)	Theoretical	$\rho_{nfpp} = \frac{\rho_l(r_{pp}+\delta)^3 + r_{pp}^3\rho_p - r_{pp}^3\rho_l}{(r_{pp}+\delta)^3}$ $\rho_{nfcc} = \frac{\rho_l(r_{cc}+\delta)^3 + r_{cc}^3\rho_p - r_{cc}^3\rho_l}{(r_{cc}+\delta)^3}$ $\rho_{nf} = \rho_{bf}(1-\varphi_{eff}) + \varphi_{cc}\rho_{nfcc} + \varphi_{pp}\rho_{nfpp}$

Montazer et al. (2018) [25]	MWCNT/H_2O, GNP/ H_2O ($0.025<\varphi<0.1$ wt%; 20 °C <T<40°C)	Experimental & RSM	$\rho_{nf}= -0.00443T^2 - 0.096\varphi T - 0.02468T + 18.40\varphi + 1000.15$ {For MWCNT/H_2O } $\rho_{nf}= -0.00518T^2 + 25.6\varphi^2 - 0.0184\varphi T + 0.01741T + 2{:}456\varphi + 999{:}886$ {For GNP/ H_2O}
Akilu et al. (2020) [27]	TiN/ H_2O-EG (60:40) ($0.25<\varphi<1.0$ vol%; 20 °C <T<40°C)	Experimental & Excel (Levenberg–Marquardt algorithm)	$\rho_{nf} = \rho_{bf}\left\{1.121\left(\frac{\varphi_p}{100}\right)^{0.01882} \times \left(\frac{T_{nf}}{333.15}\right)^{-0.04674} \times BR^{0.005495}\right\}$
Yadav et al. (2021) [26]	Al_2O_3/EG (13nm & 50nm), CuO/EG, CeO_2/EG ($0.2<\varphi<1.5$ vol%; 20 °C <T<80°C)	Experimental & RSM	$\rho_{nf}= \rho_o + A\varphi + BT$ $\rho_{nf}= 1.12809 + 0{:}02693\varphi - 0.000688095T$ {For Al_2O_3 / EG (13nm)} $\rho_{nf}= 1.128 + 0.05944\,\varphi - 0.000690293T$ {For CeO_2 / EG (25nm)}
Singh & Ghosh. (2022) [44]	AL_2O_3/DIW, GNP/DIW, MWCNT/DIW ($0.1<\varphi<1$ vol%, 30< T <80°C)	Experimental & ANN	$\rho_{nf}= \rho_{bf}(\alpha_1 + (\alpha_2 \times \varphi) + (\alpha_3 \times T) + (\alpha_4 \times T \times \varphi)$

This study addresses gaps in the existing literature by experimentally measuring the density of single and hybrid nanofluids composed of Al_2O_3, Fe_3O_4, and multi-walled carbon nanotubes (MWCNTs) in various base fluids, including water, ethylene glycol, and water-ethylene glycol mixtures. The hybrid nanofluids will be considered at temperature (10°C < T < 50°C) and nanoparticle concentrations (0 < φ < 6 vol%). Machine learning algorithms will be used to generate correlations between the nanofluids density and its independent variables i.e. temperature, and nanoparticle concentrations and percentage of ethylene glycol in base fluid. The sensitivity of the nanofluids to respective variables will be carried out . By integrating experimental measurements with advanced machine learning techniques, this research aims to establish a robust framework for accurately predicting the density of both single and hybrid nanofluids. The outcomes will not only fill critical gaps in literature but also provide practical insights for the optimization and simulation of nanofluid related design and application in thermal energy systems, paving the way for future innovations in renewable energy and advanced heat transfer technologies.

2. Materials and Methodology

2.1 Nanoparticle and morphological properties

This study employed nanofluids prepared using Aluminum (III) oxide (Al_2O_3, 20–30 nm), Iron (III) Oxide (Fe_3O_4, 20–30 nm), and Multi-Walled Carbon Nanotubes (MWCNT, <7 nm) via the two-step preparation method outlined in prior studies [45], [46]. Single nanofluids were formulated by dispersing Al_2O_3 nanoparticles in deionized water (DIW), ethylene glycol (EG), and a 50:50 mixture of DIW and EG, using Sodium Dodecyl Benzene Sulfonate (SDBS) as a surfactant. Bi-hybrid nanofluids were prepared by combining Al_2O_3 and MWCNT nanoparticles in a 60:40 ratio, dispersed in the same base fluids with Sodium Dodecyl Sulfonate (SDS) to enhance stability. Ternary hybrid nanofluids were created using Al_2O_3, MWCNT,

and Fe_3O_4 nanoparticles in a 1:1:1 ratio, dispersed in the same base fluids and stabilized with Gum Arabic (GA) to prevent agglomeration. **Table 2** summarizes the composition of the nanofluid samples considered in this study.

Different surfactants were used for the different nanofluid samples, based on stability studies reported in previous studies by this authors and other researchers who have worked on the synthesis of Al_2O_3, Fe_3O_4 , and multi-walled carbon nanotubes (MWCNTs) and their hybrids in various base fluids [14], [38], [39], [47].

The morphology of the nanoparticles was examined using a Zeiss Crossbeam 540 FEG-SEM at the University of Pretoria's Microscopy Department. Morphological images captured at a magnification of 100 KX (**Figure 1**) revealed that Al_2O_3 nanoparticles exhibited spherical shapes with cloud-like agglomerates, Fe_3O_4 displayed a combination of spherical and plate-like structures, and MWCNT showed a tubular configuration. These morphological characteristics are consistent with findings reported in existing literature.

To ensure uniform dispersion and stability, the prepared nanofluids underwent magnetic stirring for 30 minutes at a fixed speed, followed by ultrasonication for 1 hour using a Qsonica (Q-700) sonicator operating at 90% amplitude within a temperature-controlled bath maintained at 20°C. A preliminary physical inspection confirmed the stability of the nanofluids prior to further measurements.

Table 2: Composition of Nanofluid Samples

Nanofluid	Sample	Nanoparticles	Base Fluid	Surfactant
Single nanofluid	A	Al_2O_3	DIW	SDBS
	B	Al_2O_3	EG	SDBS
	C	Al_2O_3	EG-DIW	SDBS
Bi-Hybrid nanofluid	D	Al_2O_3-MWCNT	DIW	SDS
	E	Al_2O_3-MWCNT	EG	SDS
	F	Al_2O_3-MWCNT	EG-DIW	SDS
Ternary Hybrid	G	Al_2O_3-MWCNT-Fe_3O_4	DIW	GA
	H	Al_2O_3-MWCNT-Fe_3O_4	EG	GA
	I	Al_2O_3-MWCNT-Fe_3O_4	EG-DIW	GA

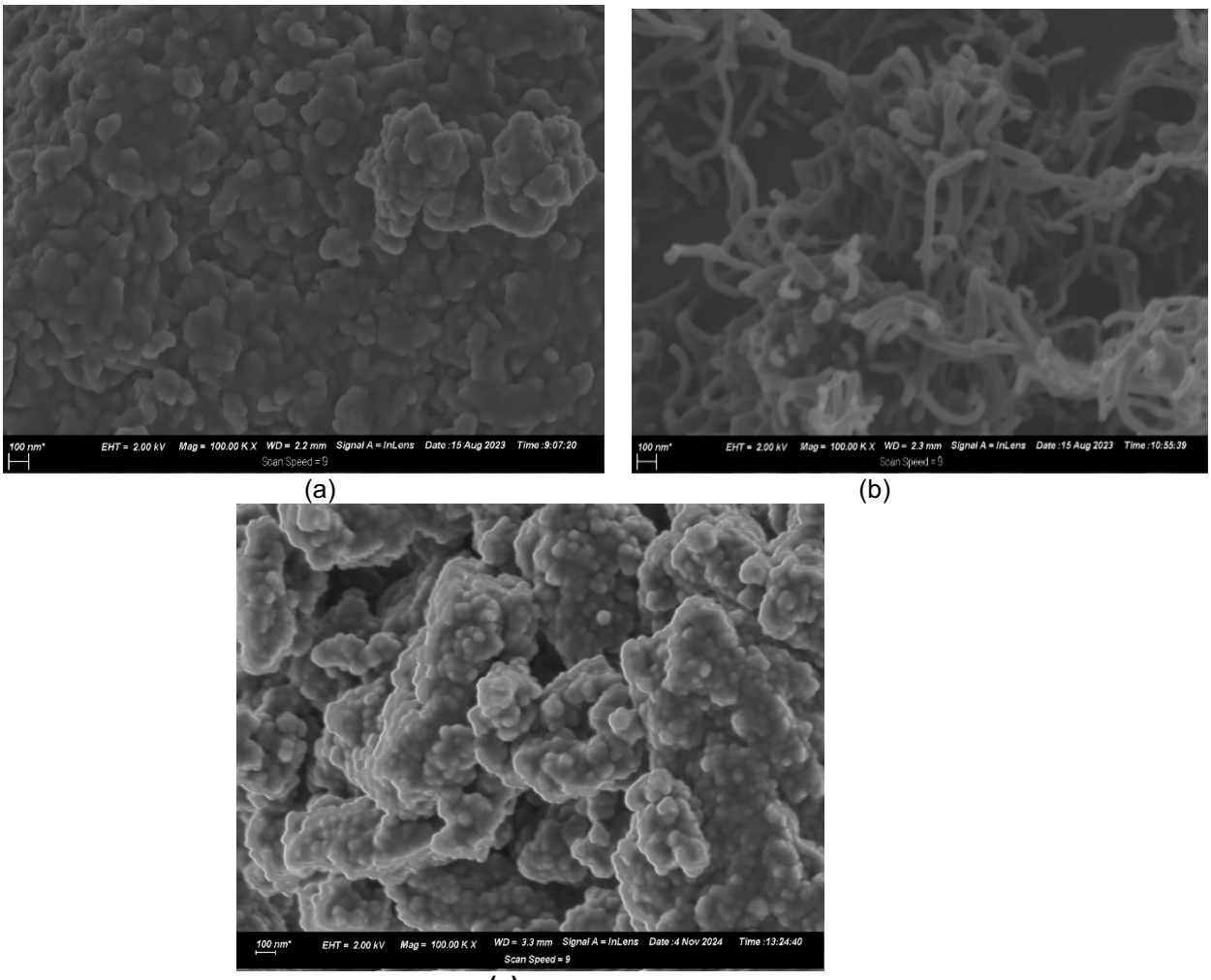

Figure 1: Morphological Image of (a) Al_2O_3 (b) MWCNT (c) Fe_3O_4 at Magnification of 100KX

2.2 Experimental Procedure

The mass of the nanofluid was measured using a Radwag PS750 R2 weighing scale, which has a sensitivity of 0.001g and linearity of ± 3.000mg. The volume of the nanofluid was accurately determined using a corked glass pycnometer in the Gay-Lussac pattern, with a fixed volume of 50.448 cm^3. The density was calculated as the ratio of the measured mass of the fully filled pycnometer to its fixed volume.

To ensure accurate and consistent density measurements of nanofluid samples, the process began with careful temperature control. The nanofluid samples were placed into small, labeled sample holders, which were then arranged on a rack and fully submerged in a thermal bath set to the desired temperature. This setup ensured the samples reached thermal equilibrium with the bath, verified using a mercury-in-glass thermometer. Once equilibrium was achieved, individual samples were removed and prepared for measurement using the pycnometer (density bottle).

The density bottle was first cleaned, dried, and weighed to determine its empty mass. It was then filled with the nanofluid sample, taking care to avoid trapping air bubbles. The neck of the bottle was filled to about one-third of its capacity, and the cork or stopper was aligned and inserted. The bottle allows the capillary tube in the stopper to fill up and excess liquid with air bubble escapes. The spill over is gently wiped off. To maintain the desired temperature, the filled bottle was re-inserted into the thermal bath. After the temperature adjustment, the bottle's outer surfaces were thoroughly dried with tissue to remove any displaced liquid.

Finally, the filled density bottle was weighed using a high-precision weighing balance to obtain the required data for density calculations. Each measurement was repeated three times for all samples under different experimental conditions (temperature and volume fraction), and the average value of the three trials was recorded as the measured density. This approach ensured consistency and minimized measurement uncertainties. All steps were carefully executed to reduce errors and prevent contamination of the bottle or sample. By strictly adhering to this methodology, the integrity and reliability of the measurements were preserved, providing accurate data for subsequent analysis. The recorded data were first processed in Excel and then visualized using Origin Plot software, as illustrated in **Figure 2**.

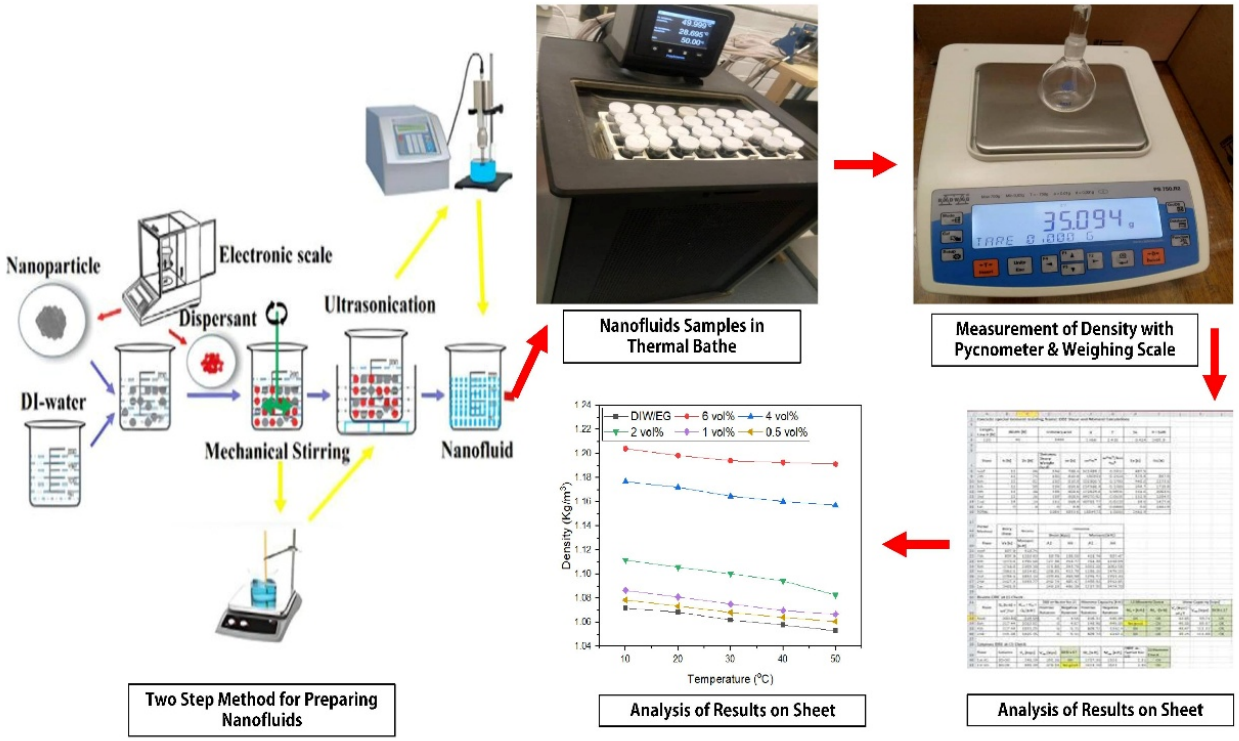

Figure 2: Schematics of Experimental Procedure

2.3 Data Reduction and Uncertainty Analysis

The density of the fluid was determined by measuring the mass and using the fixed volume of the pycnometer. The relationship between the measured mass (m), density of the nanofluid (ρ), and known volume of the pycnometer (V) is given in Equation 1.

$$\boldsymbol{\rho} = \frac{\boldsymbol{m}}{\boldsymbol{V}} \tag{1}$$

Uncertainty analysis for the measured mass and calculated density was obtained using the approach described by Moffat [48] Kline [49] and Atofarati et al. [38]. The estimation of δx_i ($\boldsymbol{\delta m}$ & $\boldsymbol{\delta V}$) for the mass and volume were accounted using both bias (b) and precision (p) errors. This analysis was carried out with the "Uncertainty" function in Python, which calculates uncertainties at a 95% confidence level. The uncertainty in mass was ± 3.17 ×10^{-3} g, while that of density was ± 2.20×10^{-5} g/cm³.

$$\boldsymbol{\delta x_i} = \left(\mathbf{b}_i^2 + \mathbf{p}_i^2\right)^{1/2} \tag{2}$$

$$\boldsymbol{\delta D} = \left\{\left(\frac{\boldsymbol{\delta D}}{\boldsymbol{\delta m}} \times \boldsymbol{\partial m}\right)^2 + \left(\frac{\boldsymbol{\delta D}}{\boldsymbol{\delta V}} \times \boldsymbol{\partial V}\right)^2\right\}^{1/2} \tag{3}$$

2.4 Machine Learning Approach

The machine learning analysis for this study was conducted using Python's Jupyter Notebook to develop predictive models and classify nanofluid density based on key independent variables: temperature, nanoparticle volume fraction, and

base fluid composition (including ethylene glycol and deionized water mixtures). The data obtained from experimental measurement was used for both regression and classification analysis following the methodologies explained in previous studies by Atofarati et al.[50] Awe et al. [51] and Adogbeji et al. [52].

The workflow began with data restructuring, cleaning and then the implementing of a linear regression model to predict nanofluid density by capturing the relationships between independent variables. To ensure robust model evaluation, the dataset was split into 80% training data and 20% testing data, with the training set used to develop predictive models and the testing set for assessing generalization performance. Model effectiveness was measured using Mean Absolute Error (MAE), R^2, Accuracy, and F1 Score.

In addition to regression modeling, a classification analysis was conducted to categorize nanofluid density using five widely recognized machine learning algorithms: Support Vector Machine (SVM), Random Forest, Logistic Regression, Gradient Boosting, and LightGBM. These models were selected due to their proven effectiveness in handling non-linear relationships, robustness to overfitting, and interpretability across engineering datasets. These analyses provided insights into the relative influence of temperature, volume fraction, and base fluid composition on nanofluid density, helping to identify key contributing factors.

3. Experimental Results

3.1 Validation of base fluid density

Prior to determining the density of the nanofluids, the measured density of the base fluids was validated against established literature data as presented in **Figure 3**. The density of deionized water was cross-referenced with values provided in the renowned textbook *Heat and Mass Transfer* by Çengel et al. [53]. The comparison revealed a perfect match, as the density-temperature graphs from both sources overlapped consistently across the temperature range.

For the ethylene glycol and deionized water mixture (50:50 by volume), the measured densities were compared with data reported by Bohne et al. [54]. The results demonstrated close alignment, with only minor deviations observed at higher temperatures. These minor discrepancies fall within acceptable experimental tolerances. Typically, **Figure 3** shows that the density of ethylene glycol was highest, followed by that of ethylene glycol-water mixture, and then De-ionized water. Also, the density of the base fluids is proportionally reduced with temperature increase.

Given the strong agreement between our measurements and the benchmark data for both deionized water and the ethylene glycol-water mixture, the validation establishes the reliability of the experimental setup. Consequently, we proceeded with the density measurements for the nanofluids.

3.2 Experimental results

The measured density of nanofluids is categorized into three systems: single nanofluids, bi-hybrid nanofluids, and ternary-hybrid nanofluids. For each case, the effects of the ethylene-glycol (EG) percentage in the base fluid (0%, 50%, and 100%) are examined. The variations in density with respect to temperature and nanoparticle volume fraction are analyzed and reported in detail.

3.2.1 Single nanofluid (Al_2O_3 nanofluids)

The density of nanofluids containing Al_2O_3 nanoparticles was determined for three base fluids: pure deionized water (DIW), ethylene glycol (EG), and a 50:50 mixture of DIW and EG. **Figure 4** illustrates the density variations for Al_2O_3/DIW, Al_2O_3/EG, and Al_2O_3/DIW-EG nanofluids as functions of temperature (10–50 °C) and nanoparticle volume fraction (0.5%, 1%, 2%, 4%, and 6%).

The experimental results revealed a nearly linear decrease in density with increasing temperature for all the nanofluid, reflecting the typical thermal expansion behavior of liquids. Among the nanofluids, the Al_2O_3/DIW nanofluids exhibited a smaller slope in the density-temperature relationship compared to Al_2O_3/EG and Al_2O_3/DIW-EG nanofluids. This suggests a more stable density response with temperature for DIW-based nanofluids.

The density of all nanofluids increased with nanoparticle volume fraction, attributed to the higher density of Al_2O_3 nanoparticles compared to the base fluids. However, the extent of density increases with volume fraction varied among the base fluids. For Al_2O_3/DIW nanofluids, the density showed consistent increases across all volume fractions, with the most pronounced effect at 6 vol%. In contrast, for Al_2O_3/EG nanofluids, significant density changes were observed only at higher volume fractions (e.g., 4 vol% and 6 vol%), while the increase was relatively minor at lower volume fractions (e.g., 0.5 vol% to 2 vol%).

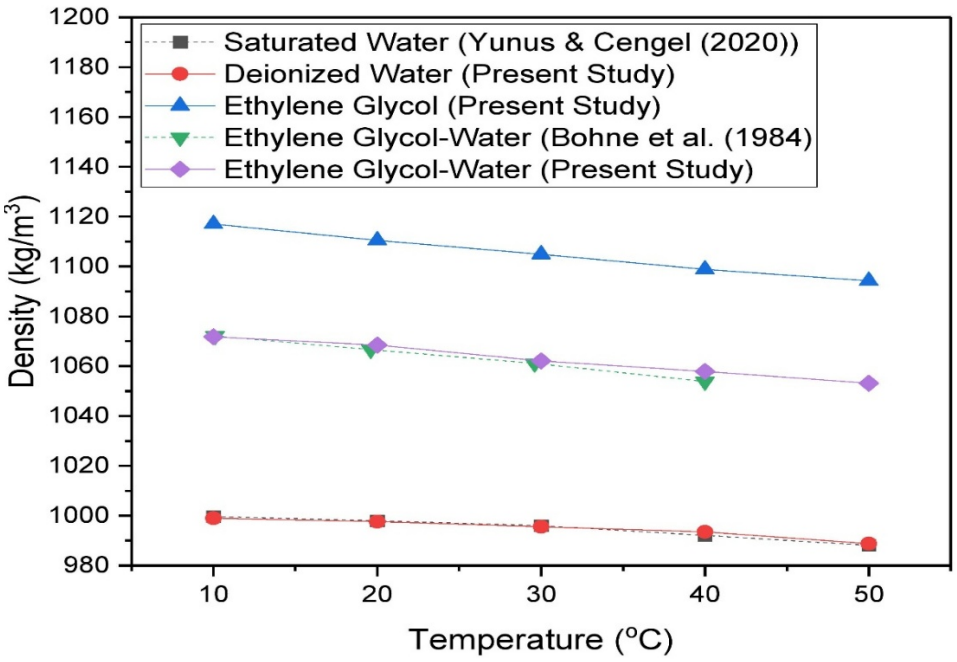

Figure 3: Validation of Measured Base Fluid Density with Literature Results

The Al_2O_3/DIW-EG nanofluids demonstrated intermediate behavior, with density values falling between those of the Al_2O_3/DIW and Al_2O_3/EG nanofluids. This trend highlights the combined effects of the two base fluids in influencing nanofluid density. Overall, the density variations of the nanofluids followed trends like those of the base fluids, decreasing with temperature and increasing with nanoparticle volume fraction. These findings are consistent with theoretical predictions and underscore the critical role of nanoparticle dispersion and base fluid properties in determining nanofluid density.

3.2.2 Bi-hybrid nanofluid (Al_2O_3-MWCNT nanofluids)

The relationship between density and temperature for Al_2O_3-MWCNT/DIW nanofluids, Al_2O_3-MWCNT/DIW-EG nanofluids, and Al_2O_3-MWCNT/EG nanofluids across a range of nanoparticle volume fractions (0 vol% < φ < 6 vol%) is presented in **Figure 5**. The density variations were evaluated as a function of temperature (10–50 °C). The results reveal distinct trends influenced by the type of base fluid and the combined contribution of Al_2O_3 and MWCNT nanoparticles.

For all base fluids, the density of the bi-hybrid nanofluids decreases approximately linearly with increasing temperature, consistent with the thermal expansion behavior typically observed in single nanofluids. This linear trend highlights the dominant influence of the base fluid's properties on the temperature-dependent behavior of the nanofluids. Additionally, the density increases with nanoparticle volume fraction, reflecting the higher density of Al_2O_3 and MWCNT nanoparticles compared to the base fluids.

The bi-hybrid nanofluids exhibit trends like single nanofluids, showing a nearly linear decrease in density as temperature increases. Additionally, density increases proportionally with rising nanoparticle volume fraction, indicating that higher concentrations of nanoparticles contribute to greater fluid density. The properties of the base fluid also play a significant role, with DIW-based nanofluids displaying the lowest density values, while EG-based nanofluids exhibit the highest densities due to the inherently higher density of ethylene glycol.

Despite these similarities, notable differences arise from the inclusion of MWCNT in the bi-hybrid system, leading to higher density values across all base fluids compared to single nanofluids. This increase is attributed to the combined mass contribution of Al_2O_3 and MWCNT nanoparticles. In DIW-based nanofluids, Al_2O_3-MWCNT nanofluids consistently exhibit higher density than single nanofluids, with this effect becoming more pronounced at higher volume fractions, such as 6 vol%.

For EG-based nanofluids, the bi-hybrid nanofluids achieve the highest density among the three base fluids, further enhanced by the inherently dense EG base fluid. Meanwhile, in DIW-EG mixture nanofluids, the density values fall between

those of DIW and EG-based nanofluids, following trends observed in single nanofluids. However, the addition of MWCNT significantly increases density compared to Al_2O_3-only nanofluids, emphasizing the impact of nanoparticle selection on nanofluid density.

The results demonstrate that bi-hybrid nanofluids exhibit superior density values compared to their single nanofluid counterparts. The synergistic effect of Al_2O_3 and MWCNT nanoparticles enhances the mass contribution and dispersion characteristics within the base fluids, leading to improved density properties. These findings underscore the potential of bi-hybrid nanofluids in applications where enhanced thermal and physical properties are critical.

In summary, the bi-hybrid nanofluids preserve the temperature-density and volume fraction-density trends of single nanofluids while introducing significant improvements, particularly at higher nanoparticle concentrations and with denser base fluids.

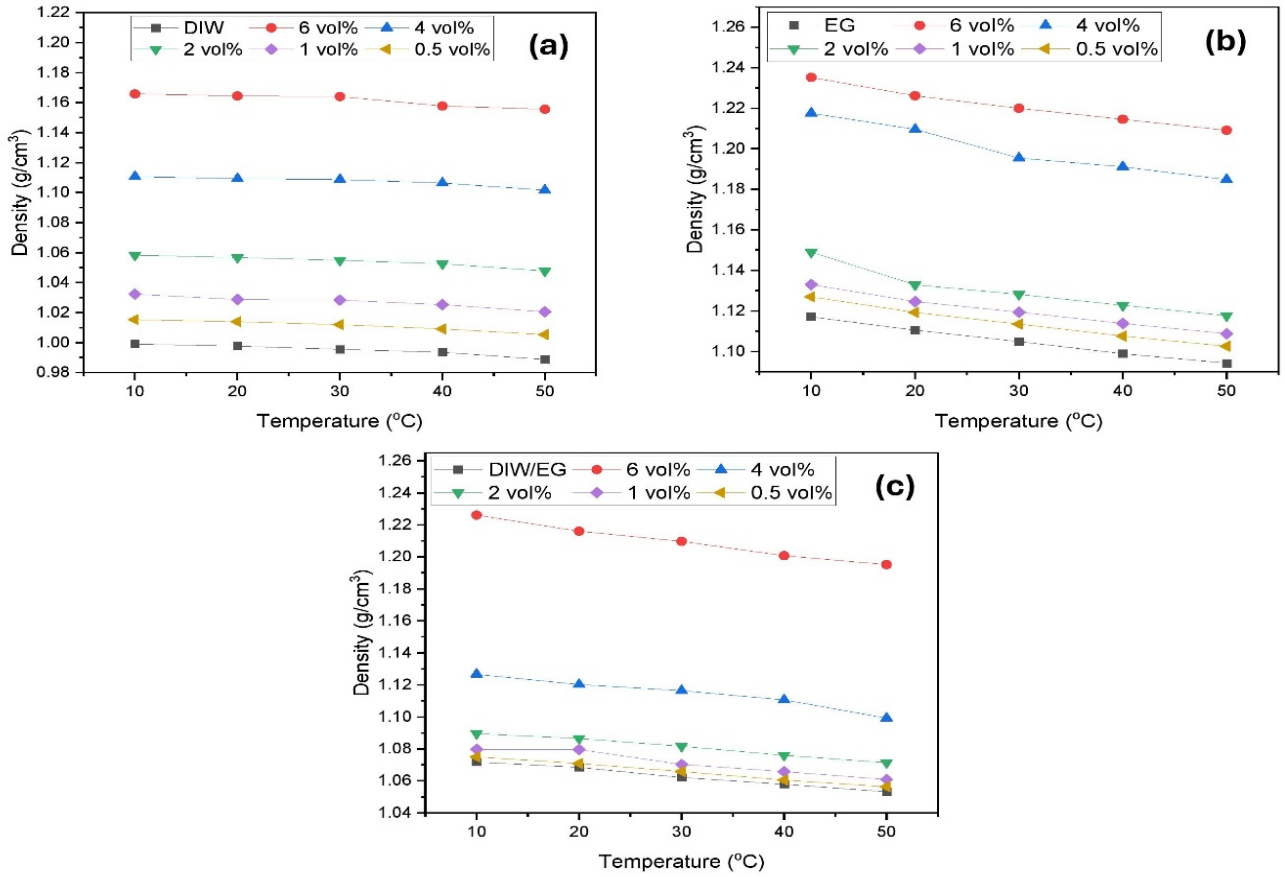

Figure 4: Experimentally Measured Density for (a) Al_2O_3/DIW Nanofluids, (b) Al_2O_3/DIW-EG Nanofluids and (c) Al_2O_3/EG Nanofluids as a Function of Temperature and Volume Fraction.

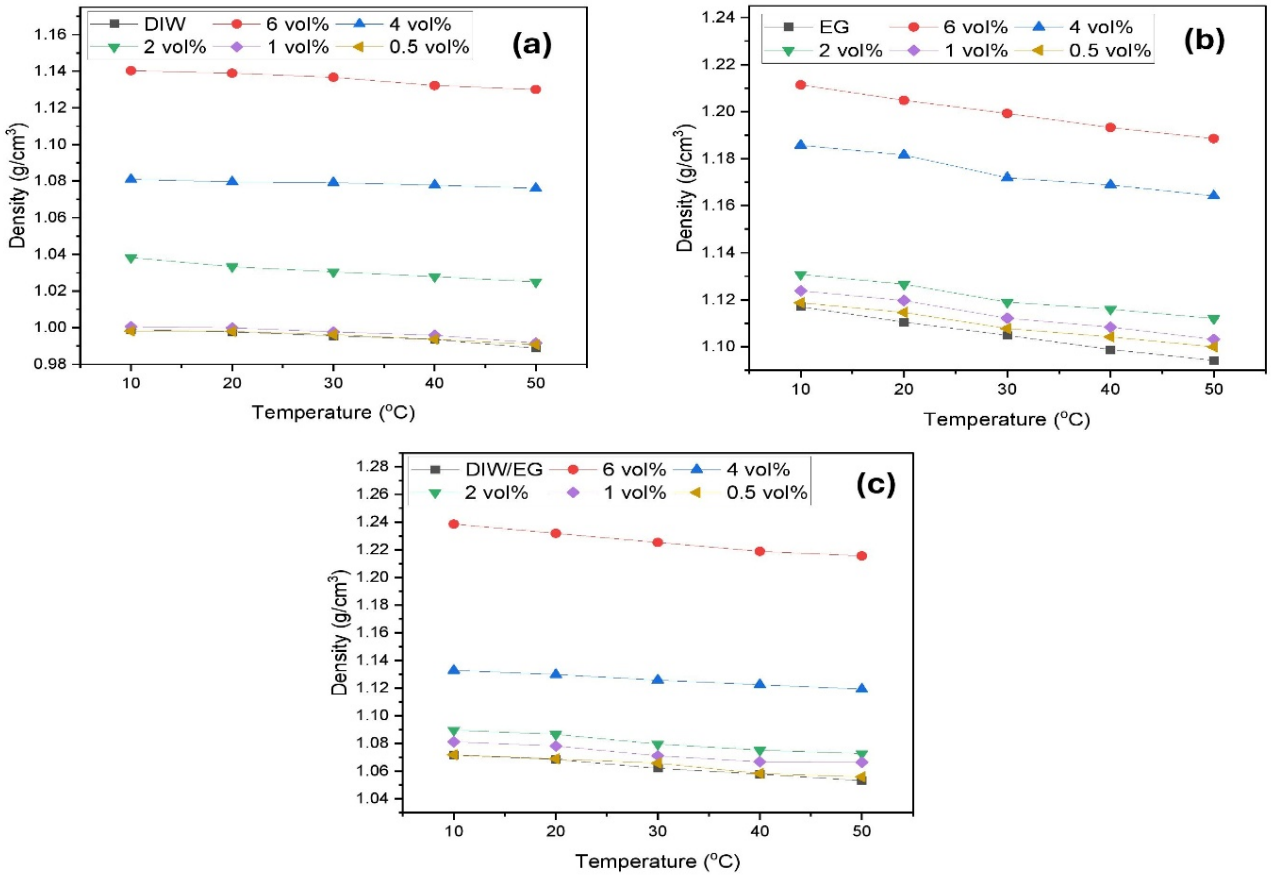

Figure 5: Experimentally Measured Density for (a) Al_2O_3-MWCNT/DIW Nanofluids, (b) Al_2O_3-MWCNT/DIW-EG Nanofluids and (c) Al_2O_3-MWCNT/EG Nanofluids as a Function of Temperature and Volume Fraction

3.2.3 Ternary nanofluids (Al_2O_3-MWCNT-Fe_3O_4 nanofluids)

Figure 6 illustrates the variation in density as a function of temperature (10–50 °C) and nanoparticle volume fractions (0.5%, 1%, 2%, 4%, and 6%) for Al_2O_3-MWCNT-Fe_3O_4 nanofluids with DIW, EG, and DIW-EG as base fluids. The inclusion of Fe_3O_4 nanoparticles in the Al_2O_3-MWCNT system introduces significant changes to the density behavior compared to single and bi-hybrid nanofluids.

The ternary-hybrid nanofluids exhibit distinct density trends across different base fluids. For all three base fluids, density decreases almost linearly with increasing temperature, a behavior consistent with the thermal expansion properties observed in single and bi-hybrid nanofluids. Additionally, an increase in nanoparticle volume fraction results in a proportional rise in density, as expected due to the higher density of the nanoparticles compared to the base fluids. Among the three systems, the density values are lowest in deionized water (DIW) due to its relatively lower density compared to ethylene glycol (EG) and DIW-EG mixtures, as shown in Figure 6a. In contrast, ternary-hybrid nanofluids prepared with EG as the base fluid exhibit the highest density values across all volume fractions, attributed to the inherently higher density of EG (Figure 6b). The density of nanofluids using the DIW-EG mixture as the base fluid falls between the two extremes, reflecting the combined influence of DIW and EG properties (Figure 6c). Despite variations in composition, a linear relationship between density and temperature remains a common feature across all nanofluid types. Moreover, density consistently increases with higher nanoparticle volume fractions, regardless of the level of hybridization or the choice of base fluid.

The introduction of Fe_3O_4 nanoparticles in the ternary-hybrid system significantly enhances the density values compared to single and bi-hybrid nanofluids, primarily due to the high density of Fe_3O_4. For DIW-based ternary-hybrid nanofluids, the

density values surpass those of single and bi-hybrid systems at all volume fractions, with the improvement most pronounced at higher concentrations (e.g., 6 vol%). Similarly, the EG- and DIW-EG-based ternary-hybrid nanofluids also achieve higher density values than their single and bi-hybrid counterparts, underscoring the additive effect of Fe_3O_4 nanoparticles.

The density values of ternary-hybrid nanofluids show a marked improvement over single and bi-hybrid systems across all base fluids. In DIW-based nanofluids, there is a noticeable enhancement in density, effectively bridging the gap with the higher-density EG systems observed in single and bi-hybrid cases. For EG-based nanofluids, the highest density values are maintained, with further amplification due to the ternary-hybrid nanoparticle configuration. Similarly, nanofluids based on the DIW-EG mixture exhibit consistently higher density values than their bi-hybrid counterparts, highlighting the synergistic effect of Fe_3O_4 in the hybrid system

The ternary-hybrid nanofluids exhibit significant density enhancements compared to single and bi-hybrid systems, attributable to the combined mass contribution of Al_2O_3, MWCNT, and Fe_3O_4 nanoparticles. The choice of base fluid plays a critical role in determining the absolute density values, with EG-based nanofluids achieving the highest and DIW-based nanofluids the lowest. These results emphasize the impact of nanoparticle hybridization and base fluid selection on optimizing the density of nanofluids, which is crucial for tailoring their properties for specific thermal management applications.

The density of ternary-hybrid nanofluids containing Al_2O_3, MWCNT, and Fe_3O_4 nanoparticles was evaluated for DIW, EG, and DIW-EG base fluids. Figure 6 illustrates the density variations as functions of temperature (10–50 °C) and nanoparticle volume fractions (0.5%, 1%, 2%, 4%, and 6%).

Impact of Temperature

Ternary-hybrid nanofluids exhibited a nearly linear decrease in density with increasing temperature, a trend consistent with single and bi-hybrid nanofluids. The temperature-density relationship was primarily influenced by the properties of the base fluid. DIW-based nanofluids displayed the lowest density values across the temperature range, while EG-based nanofluids achieved the highest densities due to the inherently dense nature of EG. Meanwhile, DIW-EG-based nanofluids exhibited intermediate density values, reflecting the combined influence of DIW and EG properties.

Impact of Volume Fraction

The incorporation of Fe_3O_4 nanoparticles significantly increased the density of ternary-hybrid nanofluids compared to single and bi-hybrid systems. In DIW-based nanofluids, density values surpassed those of single and bi-hybrid systems across all volume fractions, with the most notable enhancement observed at 6 vol%. For EG-based nanofluids, the ternary-hybrid configuration maintained the highest density values, further reinforced by the inherently dense EG base fluid. Similarly, DIW-EG-based nanofluids exhibited consistently higher density values than their bi-hybrid counterparts, demonstrating the additive effect of Fe_3O_4 nanoparticles in enhancing overall density.

The results highlight the combined mass contributions of Al_2O_3, MWCNT, and Fe_3O_4 nanoparticles, which significantly enhance density properties. The choice of base fluid critically determines the absolute density values, with EG-based systems achieving the highest and DIW-based systems the lowest.

4. Machine Learning Results

4.1 Predictive model performance

The machine learning analysis using linear regression models for Al_2O_3 nanofluids, Al_2O_3-MWCNT nanofluids, and Al_2O_3-MWCNT-Fe_3O_4 nanofluids demonstrated a strong correlation between actual and predicted density values, as summarized in **Figures 7, 8, and 9**. These models employed temperature (T), nanoparticle volume fraction (φ), and the percentage composition of ethylene glycol in the base fluid (BF) as independent variables to predict nanofluid density (ρ). The correlations derived are summarized in **Table 3**.

Al_2O_3 Nanofluids

For Al_2O_3-based nanofluids, the linear regression models achieved high predictive accuracy, as evidenced by the R^2 values and low Mean Squared Error (MSE). Sample A (DIW-based) exhibited an R^2 of 0.99897 and a minimal MSE of 0.0000035, as shown in **Figure 7(a)**, indicating excellent model performance. For Sample B (EG-based) and Sample C (DIW-EG mixture), the R^2 values were 0.96271 and 0.89990, respectively, with slightly higher errors due to the increased complexity of the fluid systems (**Figure 7(b) and 7(c)**). These models achieved accuracy levels of 99.9%, 96.3%, and 90.0% for Samples A, B, and C, respectively, confirming their reliability in estimating nanofluid densities.

A generalized model encompassing all three base fluids was developed, incorporating the ethylene glycol percentage in DIW as the BF variable, as shown in **Figure 7(d)**. This generalized model achieved an accuracy of 96.05% with an MSE of 0.0001605, highlighting its capability to predict density variations across diverse base fluids.

Al_2O_3-MWCNT Nanofluids

For Al_2O_3-MWCNT nanofluids, the models effectively captured the relationship between density and the independent variables, achieving R^2 values of 0.98250, 0.96900, and 0.91399 for Samples D, E, and F, respectively, as illustrated in **Figures 8(a), 8(b), and 8(c)**. The corresponding accuracy levels were 98.3%, 96.9%, and 91.4%, indicating reliable performance across different base fluids.

A generalized model for these nanofluids, shown in **Figure 8(d)**, used BF as an independent variable and achieved an accuracy of 93.49% with an MSE of 0.0002732. This demonstrates the model's ability to predict density for various base fluid compositions effectively.

Al_2O_3-MWCNT-Fe_3O_4 Nanofluids

In the case of Al_2O_3-MWCNT-Fe_3O_4 nanofluids, the regression models provided high predictive accuracy, with R^2 values of 0.9826, 0.9706, and 0.9805 for Samples G, H, and I, respectively, as depicted in **Figures 9(a), 9(b), and 9(c).** These models achieved negligible MSE values, highlighting their robustness in handling complex nanofluid systems.

A generalized model for Al_2O_3-MWCNT-Fe_3O_4 nanofluids, shown in **Figure 9(d)**, incorporated BF as a variable and achieved an accuracy of 88.80% with an MSE of 0.0003890. This result reflects the model's capability to adapt to diverse base fluid compositions while maintaining reasonable predictive performance.

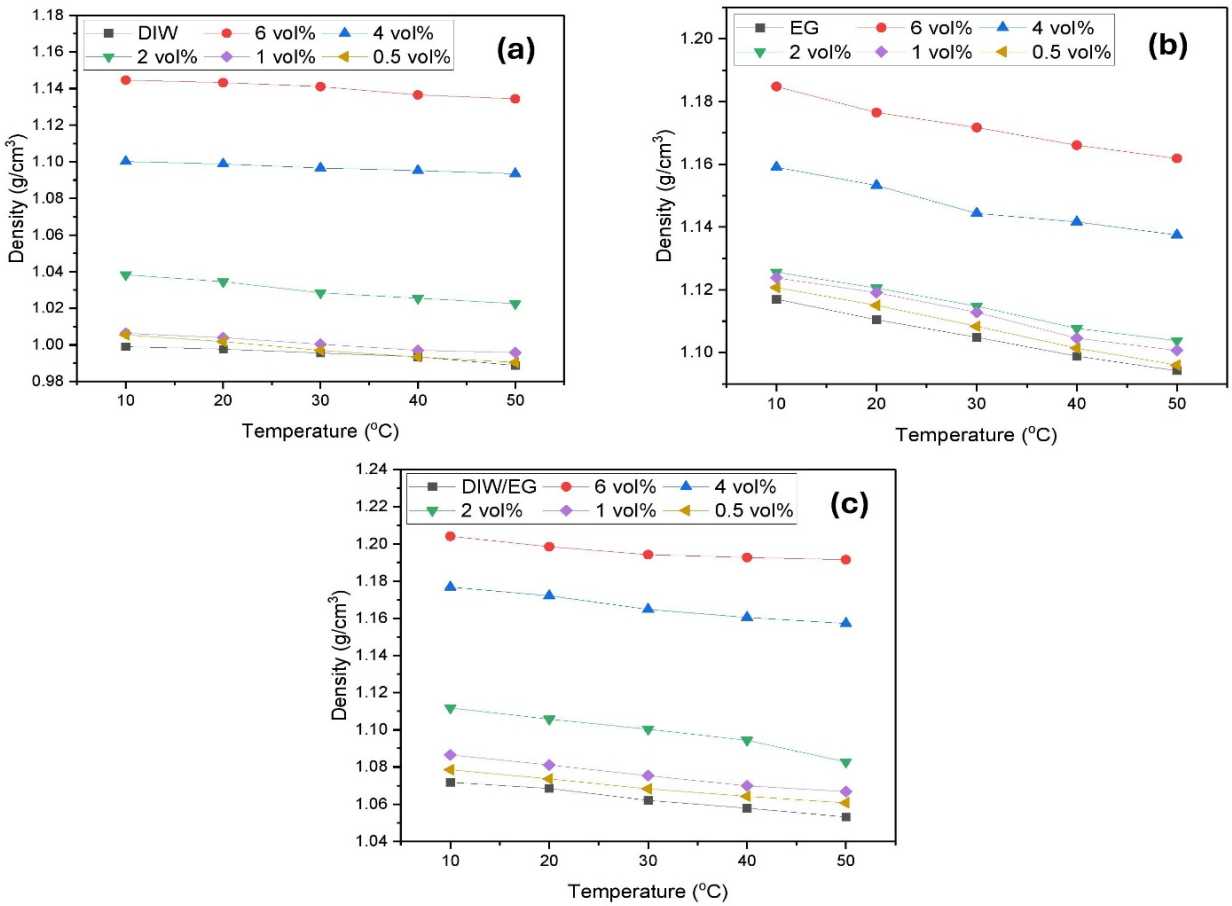

Figure 6: Experimentally Measured Density for (a) Al_2O_3-MWCNT- Fe_3O_4 /DIW Nanofluids, (b) Al_2O_3-MWCNT- Fe_3O_4 /DIW-EG Nanofluids and (c) Al_2O_3-MWCNT- Fe_3O_4 /EG Nanofluids as a Function of Temperature and Volume Fraction

Table 3: Summary of Density Model/Correlation for this study

Sample	Nanofluids	Obtained Predictive Model	Accuracy	Modified Pak & Cho model
A	Al_2O_3/DIW (SDBS)	$\rho = -0.0002T + 0.0275\varphi + 1.0050$	99.9%	$\rho_{nf} = \rho_{bf}\varphi_{bf} + \rho_{np}\varphi_{np}$ Where: $\varphi_{bf} + \varphi_{np} = 1$
B	Al_2O_3/EG (SDBS)	$\rho = -0.0007T + 0.0208\varphi + 1.1213$	96.3%	$\rho_{nf} = \rho_{bf}\varphi_{bf} + \rho_{np}\varphi_{np}$
C	Al_2O_3/DIW-EG (SDBS)	$\rho = -0.0006T + 0.0231\varphi + 1.0656$	90.0%	$\rho_{nf} = \sum_{i=1}^{2}\rho_{bf_i}\varphi_{bf_i} + \rho_{np}\varphi_{np}$ Where: $\sum_{i=1}^{2}\varphi_{bf_i} + \varphi_{np} = 1$
A/B/C	Al_2O_3 Nanofluid (BF indicating %EG in DIW)	$\rho = -0.0005T + 0.0238\varphi + 0.089BF + 1.0195$	96.1%	$\rho_{nf} = \sum_{i=1}^{n}\rho_{bf_i}\varphi_{bf_i} + \rho_{np}\varphi_{np}$
D	Al_2O_3-MWCNT/DIW (SDS)	$\rho = -0.0002T + 0.0246\varphi + 0.9902$	98.3%	$\rho_{nf} = \rho_{bf}\varphi_{bf} + \sum_{i=1}^{2}\rho_{np_i}\varphi_{np_i}$ Where: $\varphi_{bf} + \sum_{i=1}^{2}\varphi_{np_i} = 1$
E	Al_2O_3-MWCNT /EG (SDS)	$\rho = -0.0005T + 0.0169\varphi + 1.1150$	96.9%	$\rho_{nf} = \rho_{bf}\varphi_{bf} + \sum_{i=1}^{2}\rho_{np_i}\varphi_{np_i}$

F	Al_2O_3-MWCNT/DIW-EG (SDS)	$\rho = -0.0004T + 0.0262\varphi + 1.0600$	91.4%	$\rho_{nf} = \sum_{i=1}^{2} \rho_{bf_i} \varphi_{bf_i} + \sum_{i=1}^{2} \rho_{np_i} \varphi_{np_i}$ Where: $\sum_{i=1}^{2} \varphi_{bf_i} + \sum_{i=1}^{2} \varphi_{np_i} = 1$
D/E/F	Al_2O_3-MWCNT	$\rho = -0.0004T + 0.0226\varphi + 0.0983BF + 1.0059$	93.5%	$\rho_{nf} = \sum_{i=1}^{n} \rho_{bf_i} \varphi_{bf_i} + \sum_{i=1}^{n} \rho_{np_i} \varphi_{np_i}$
G	Al_2O_3-MWCNT-Fe_3O_4 /DIW (GA)	$\rho = -0.0003T + 0.0261\varphi + 0.9934$	98.3%	$\rho_{nf} = \rho_{bf} \varphi_{bf} + \sum_{i=1}^{3} \rho_{np_i} \varphi_{np_i}$ Where: $\varphi_{bf} + \sum_{i=1}^{3} \varphi_{np_i} = 1$
H	Al_2O_3-MWCNT- Fe_3O_4 /EG (GA)	$\rho = -0.0006T + 0.0115\varphi + 1.1182$	97.1%	$\rho_{nf} = \rho_{bf} \varphi_{bf} + \sum_{i=1}^{3} \rho_{np_i} \varphi_{np_i}$
I	Al_2O_3-MWCNT-Fe_3O_4 /DIW-EG (GA)	$\rho = -0.0005T + 0.0240\varphi + 1.0722$	98.1%	$\rho_{nf} = \sum_{i=1}^{2} \rho_{bf_i} \varphi_{bf_i} + \sum_{i=1}^{3} \rho_{np_i} \varphi_{np_i}$ Where: $\sum_{i=1}^{2} \varphi_{bf_i} + \sum_{i=1}^{3} \varphi_{np_i} = 1$
G/H/I	Al_2O_3-MWCNT- Fe_3O_4	$\rho = -0.0005T + 0.0205\varphi + 0.0822BF + 1.0196$	88.8%	$\rho_{nf} = \sum_{i=1}^{n} \rho_{bf_i} \varphi_{bf_i} + \sum_{i=1}^{n} \rho_{np_i} \varphi_{np_i}$

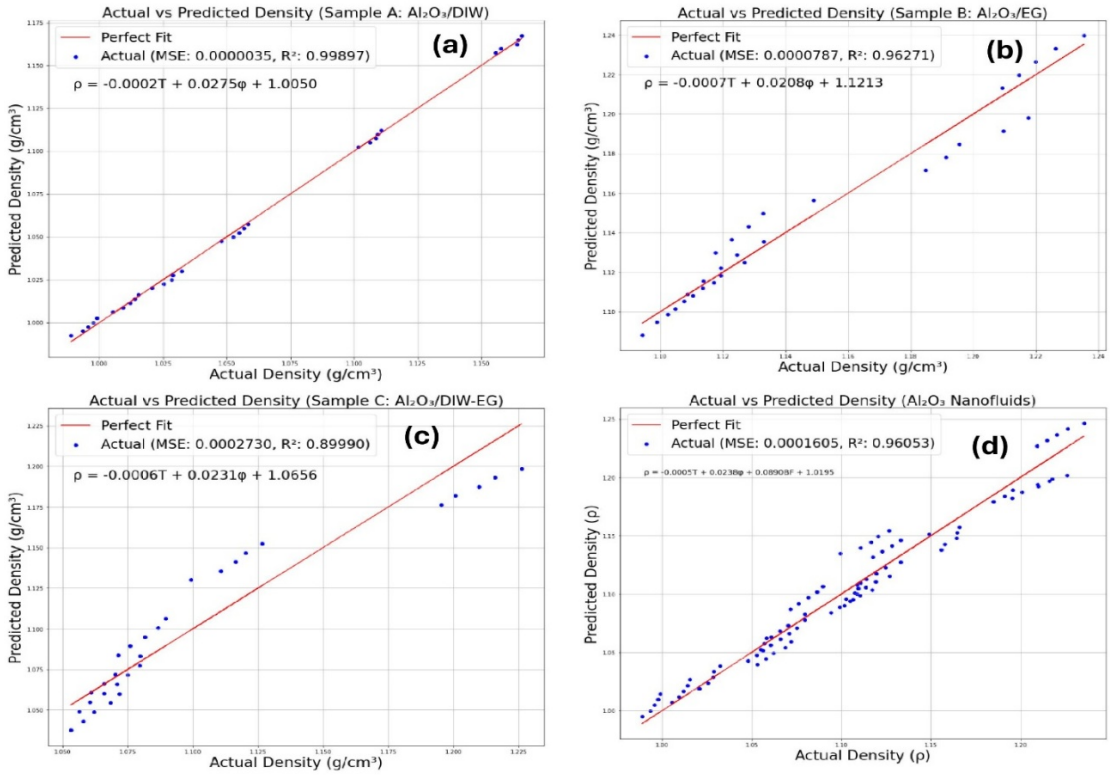

Figure 7: Predicted Correlations for Al_2O_3 Nanofluids and Their Performance

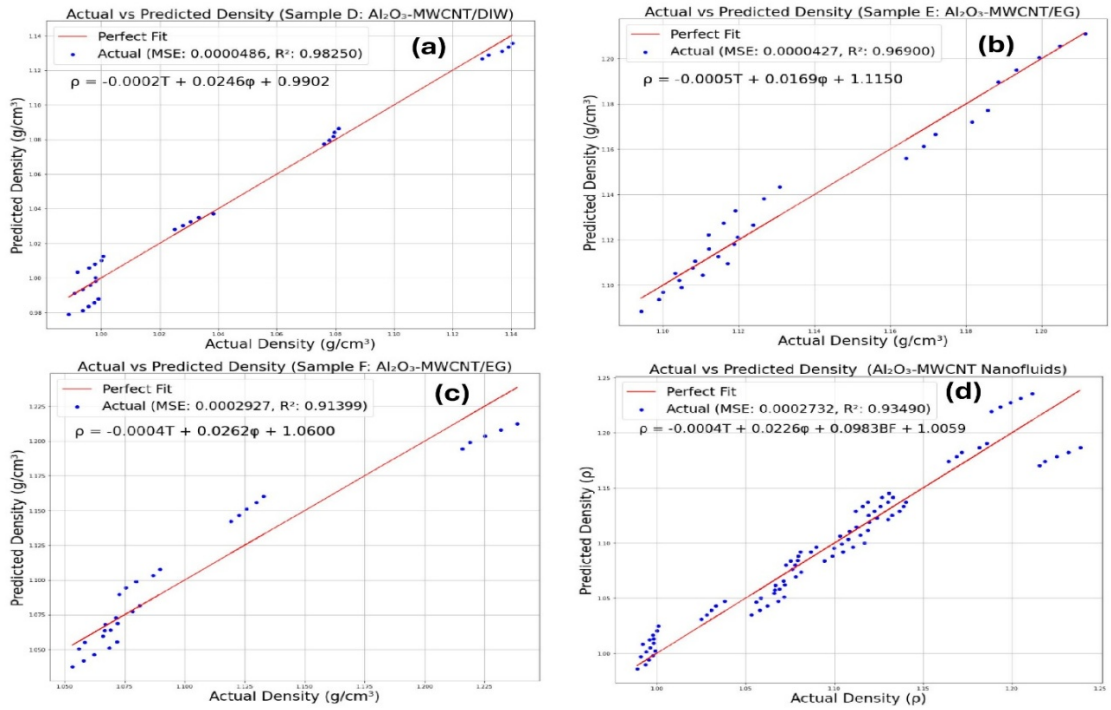

Figure 8: Predicted Correlations for Al_2O_3-MWCNT Nanofluids and Their Performance

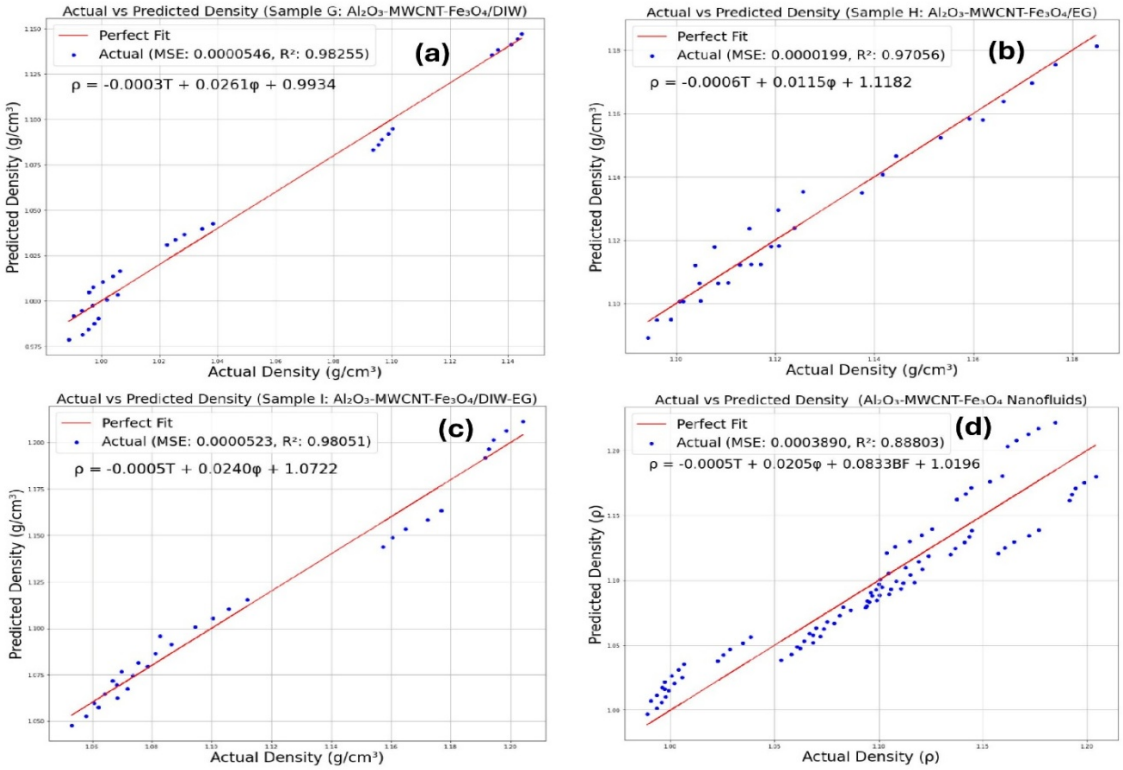

Figure 9: Predicted Correlations for Al_2O_3-MWCNT-Fe_3O_4 Nanofluids and Their Performance

4.2 Classification and feature importance model analysis

Machine learning models have become indispensable tools for analyzing complex datasets, such as those involving Al_2O_3-based nanofluids. By leveraging metrics like Mean Absolute Error (MAE), R^2, Accuracy, and F1-Score, these models provide a comprehensive evaluation of predictive performance. Higher accuracy and F1-Score signify robust classification capabilities, while lower MAE and higher R^2 indicate improved predictive precision and data fit. This study evaluates the performance of five machine learning models—Support Vector Machine (SVM) with a linear kernel (C=0.1), Random Forest, Logistic Regression, Gradient Boosting, and LightGBM—and analyzes feature importance using the best-performing models for three types of nanofluids: single, bi-hybrid, and tri-hybrid.

4.2.1 Single Al_2O_3 Nanofluids

The classification results for single Al_2O_3 nanofluids, visualized in **Figure 10** and detailed in **Table 4**, reveal that Random Forest, Logistic Regression, Gradient Boosting, and LightGBM achieved high accuracies (~0.9444) and strong predictive metrics (MAE = 0.0556, R^2 = 0.7778, F1-Score = 0.9474 to 0.9524). These results underline their reliability in predicting nanofluid density. In contrast, SVM demonstrated slightly lower performance, with an accuracy of 0.8889, MAE of 0.1111, R^2 of 0.5556, and F1-Score of 0.8889.

Figure 11 presents the feature importance analysis for Random Forest, Logistic Regression, and LightGBM. The analysis identified volume fraction as the most significant feature influencing density, followed by base fluid composition (%EG), with temperature having minimal impact. This consistency across models underscores the critical role of volume fraction in determining the behavior of Al_2O_3 nanofluids.

Table 4: Evaluation Metrics for Models used to Predict Al_2O_3 Nanofluids Data

Model	MAE	R2	Accuracy	F1-Score
SVM (Linear, C=0.1)	0.111111	0.55	0.888889	0.888889
Random Forest	0.055556	0.775	0.944444	0.947368
Logistic Regression	0.055556	0.775	0.944444	0.947368
Gradient Boosting	0.055556	0.775	0.944444	0.952381
LightGBM	0.055556	0.775	0.944444	0.952381

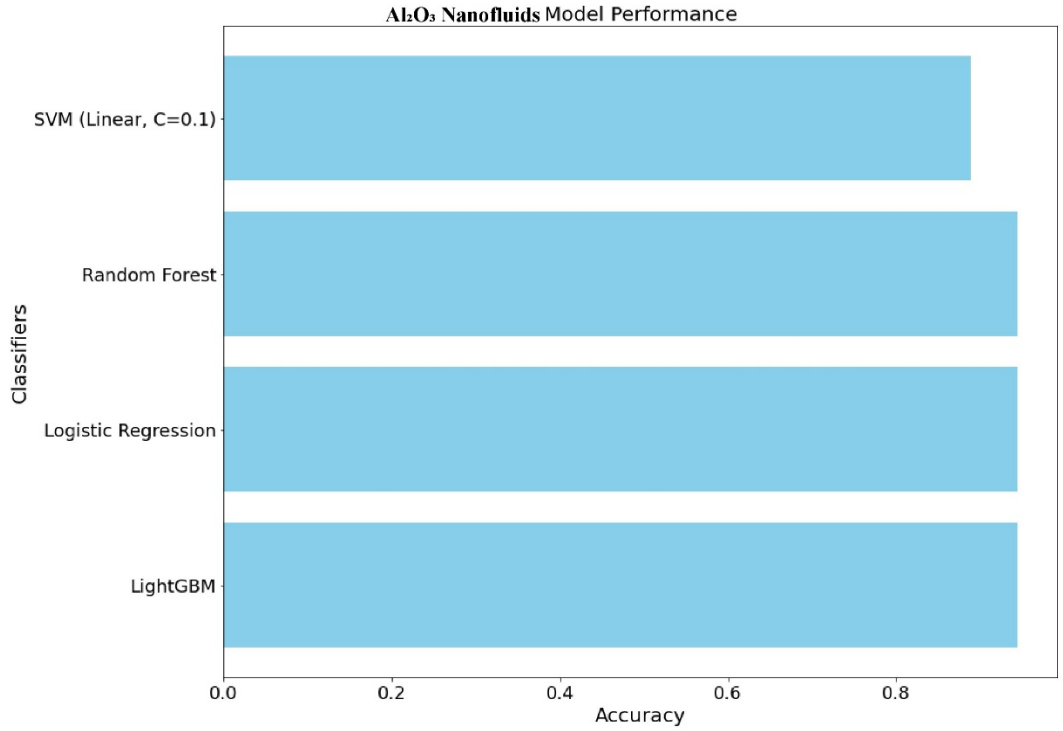

Figure 10: Models' Accuracy Plot for Al_2O_3 Nanofluids Data

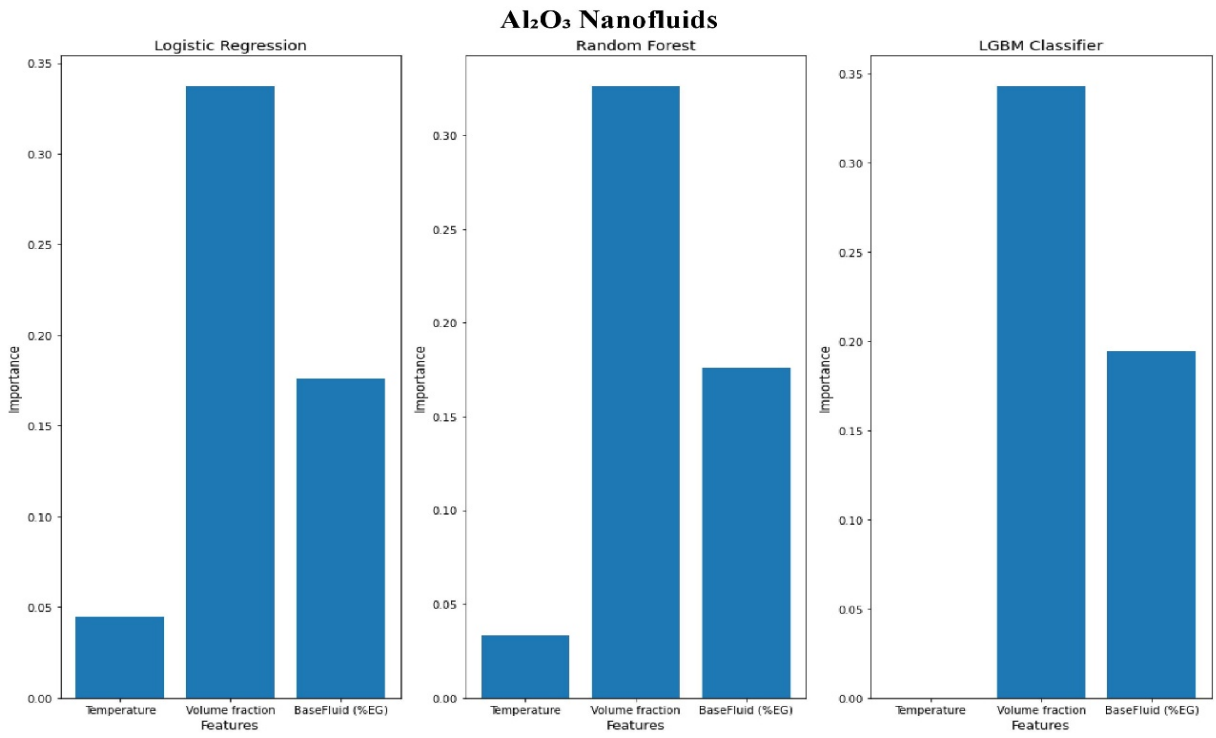

Figure 11: Density's Variable Sensitivity Plot for Al_2O_3 Nanofluids

4.2.2 Bi-Hybrid Al_2O_3-MWCNT Nanofluids

The performance of the models for bi-hybrid Al_2O_3-MWCNT nanofluids, as summarized in **Table 5** and illustrated in **Figure 12**, highlights Random Forest as the best-performing model, achieving perfect metrics (Accuracy, R^2, and F1-Score = 1, MAE = 0). Logistic Regression and Gradient Boosting also showed strong results, with accuracies of 0.9444, MAE of 0.0556, and F1-Score of 0.9474, demonstrating their reliability as alternatives to Random Forest.

SVM exhibited moderate performance, achieving an accuracy of 0.8889, F1-Score of 0.8889, MAE of 0.1111, and R^2 of 0.5556, indicating its limited ability to fully capture dataset variance. LightGBM underperformed compared to the other models, with the lowest accuracy (0.8333) and F1-Score (0.8421), and the highest MAE (0.1667), suggesting it may require further optimization. The analysis of the feature importance, shown in **Figure 13**, confirmed the dominant influence of volume fraction and base fluid composition on density prediction, while temperature maintained minimal impact.

Table 5: Evaluation Metrics for Models used to Predict Al_2O_3-MWCNT Nanofluids Data

Model	MAE	R2	Accuracy	F1-Score
SVM (Linear, C=0.1)	0.111111	0.555556	0.888889	0.888889
Random Forest	0	1	1	1
Logistic Regression	0.055556	0.777778	0.944444	0.947368
Gradient Boosting	0.055556	0.777778	0.944444	0.947368
LightGBM	0.166667	0.333333	0.833333	0.842105

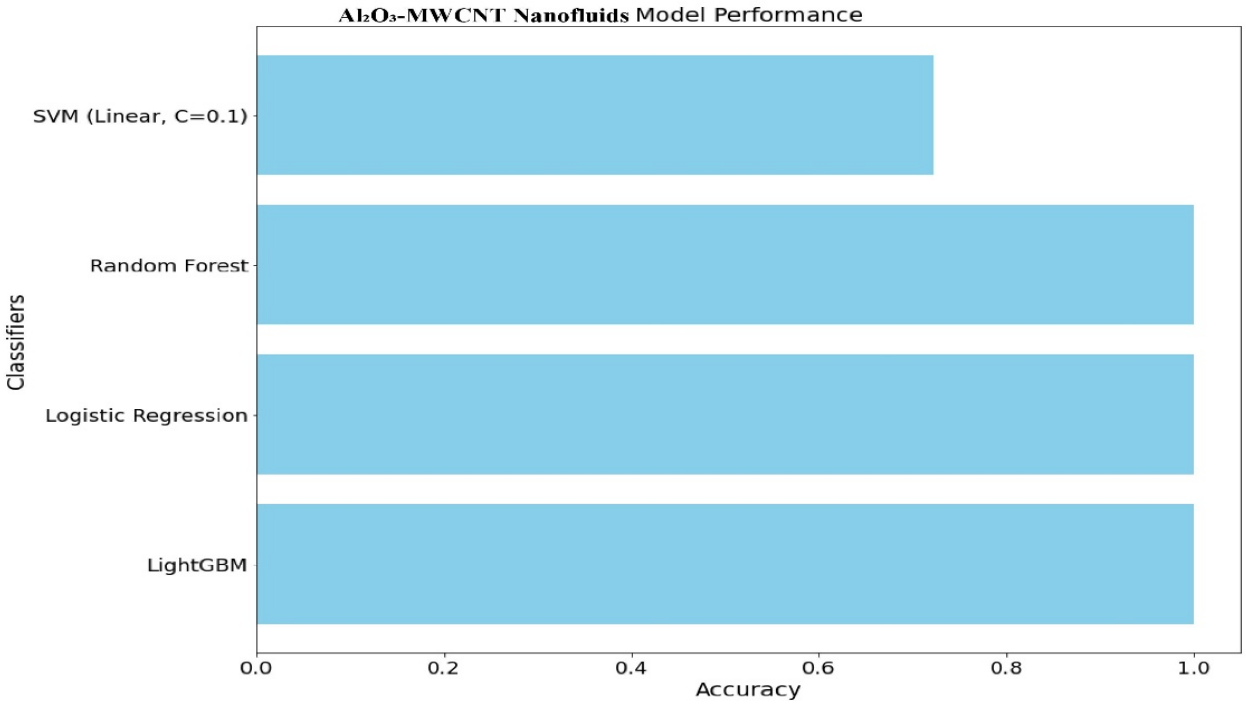

Figure 12: Models' Accuracy Plot for Al_2O_3-MWCNT Nanofluids Data

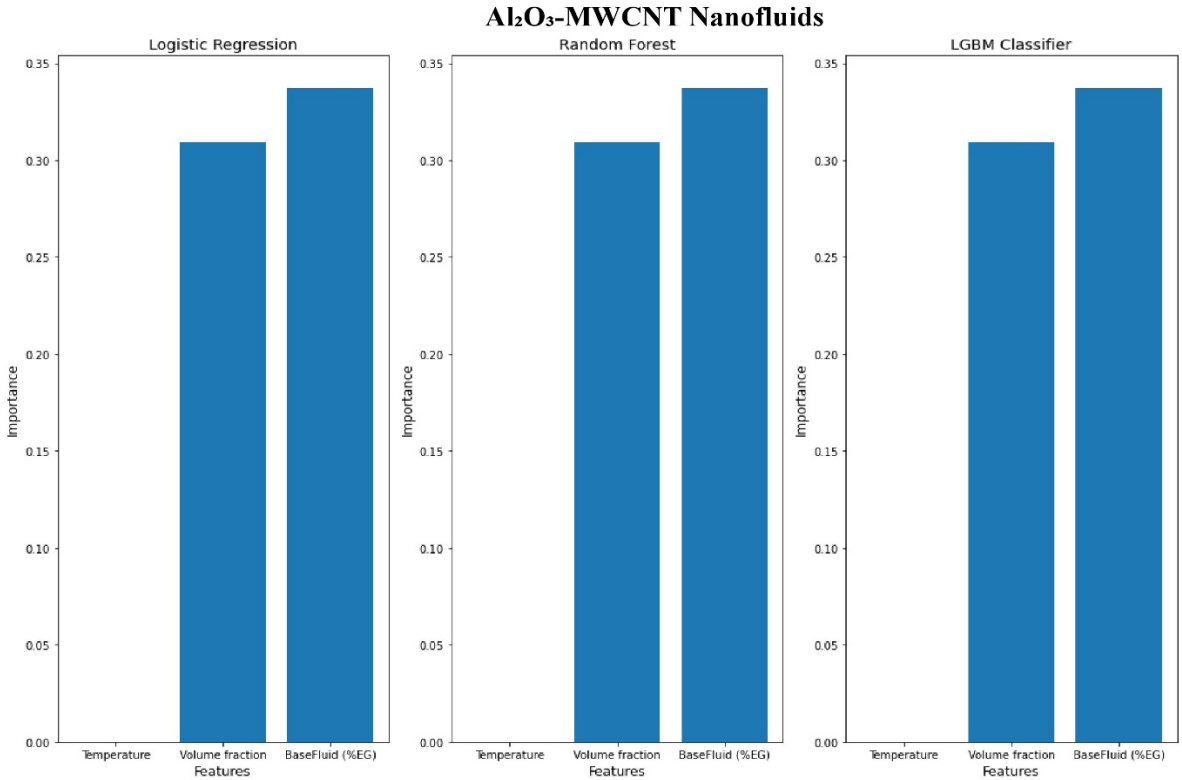

Figure 13: Density's Variable Sensitivity Plot for Al_2O_3-MWCNT Nanofluids

4.2.3 Tri-Hybrid Al_2O_3-MWCNT-Fe_3O_4 Nanofluids

The classification results for tri-hybrid Al_2O_3-MWCNT-Fe_3O_4 nanofluids, depicted in **Figure 14** and detailed in **Table 6**, further validate Random Forest as the top-performing model with perfect metrics (Accuracy, R^2, and F1-Score = 1, MAE = 0). Logistic Regression and Gradient Boosting achieved comparable results, with accuracies of 0.9444, MAE of 0.0556, and F1-Score of 0.9474. SVM displayed moderate performance, with an accuracy of 0.8889 and R^2 of 0.5556, while LightGBM showed the weakest performance (Accuracy = 0.8333, MAE = 0.1667, F1-Score = 0.8421).

Figure 15 highlights the feature importance analysis for Logistic Regression, Random Forest, and SVM, reaffirming volume fraction as the most critical variable, followed by base fluid composition. Unlike in the previous datasets, temperature showed a slightly more significant effect on density prediction, emphasizing its nuanced role in the Al_2O_3-MWCNT-Fe_3O_4 dataset.

Across all nanofluids, Random Forest consistently outperformed other models, demonstrating exceptional predictive accuracy and robustness. Logistic Regression and Gradient Boosting also emerged as reliable alternatives, while SVM and LightGBM were comparatively less effective. The feature importance analysis consistently identified volume fraction as the most influential factor, followed by base fluid composition, with temperature playing a secondary role. These findings underscore the critical role of ensemble-based machine learning models and key features like volume fraction in predicting nanofluid density, offering a robust framework for optimizing nanofluid properties through predictive modeling.

Table 6: Evaluation Metrics for the Modelling of Al_2O_3-MWCNT- Fe_3O_4 Nanofluids

Model	MAE	R2	Accuracy	F1-Score
SVM (Linear, C=0.1)	0.111111	0.555556	0.888889	0.888889
Random Forest	0	1	1	1
Logistic Regression	0.055556	0.777778	0.944444	0.947368
Gradient Boosting	0.055556	0.777778	0.944444	0.947368
LightGBM	0.166667	0.333333	0.833333	0.842105

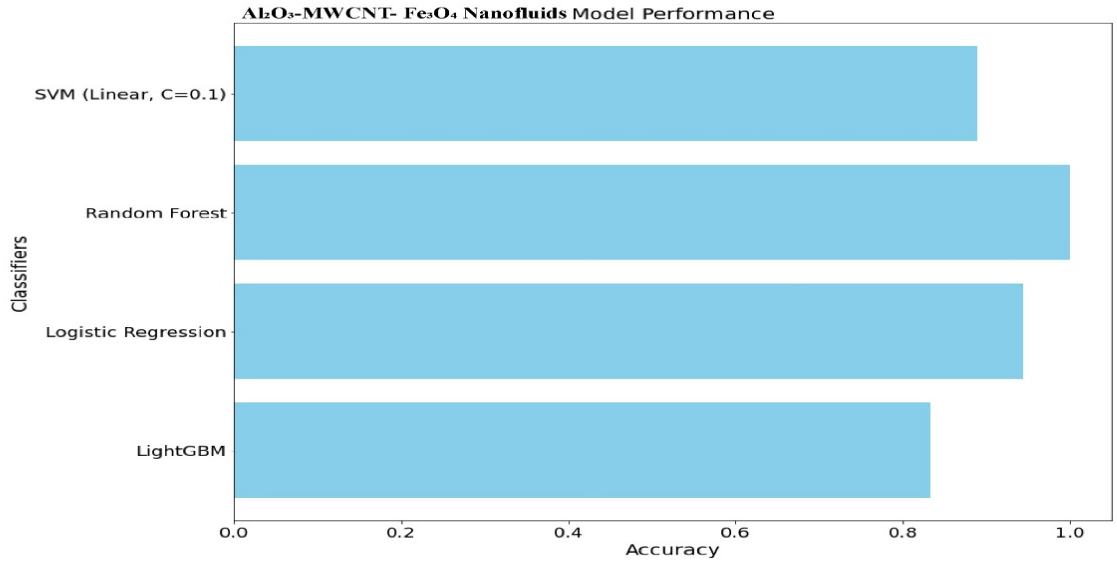

Figure 14: Models' Accuracy Plot for Al_2O_3-MWCNT- Fe_3O_4 Nanofluids Data

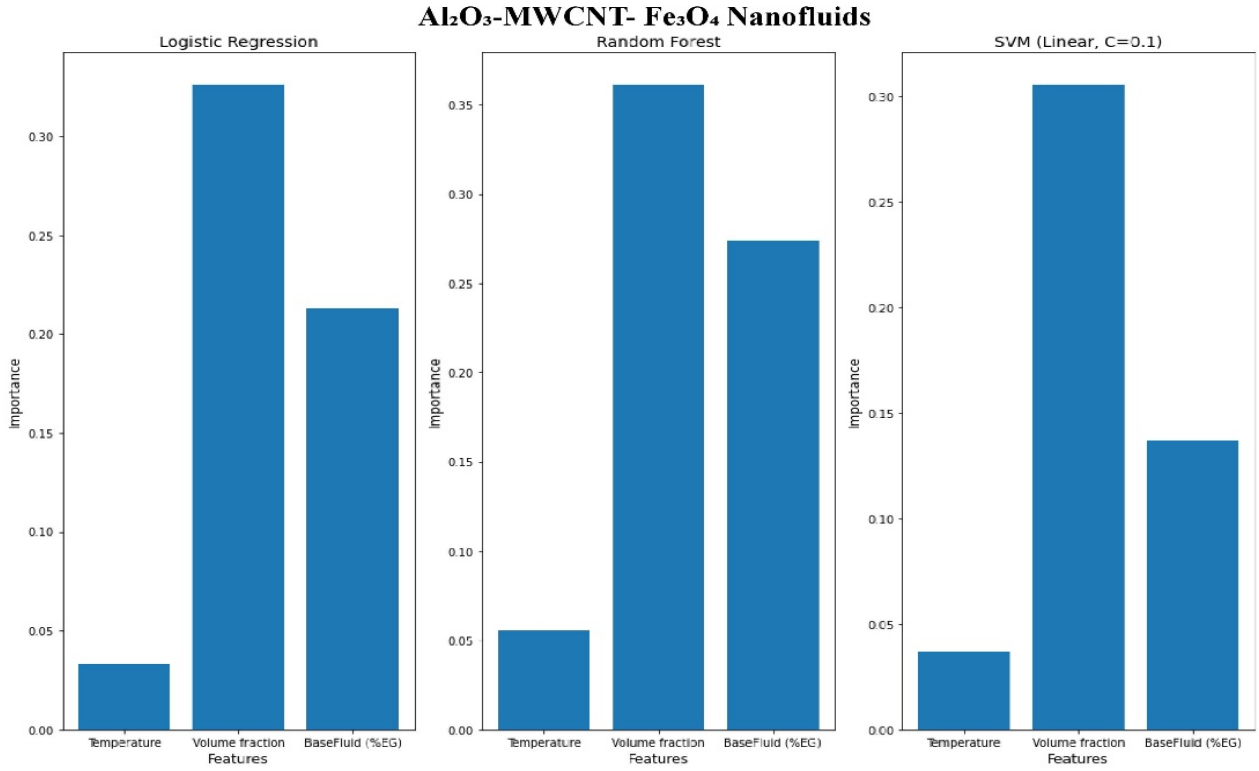

Figure 15: Density's Variable Sensitivity Plot For Al_2O_3-MWCNT- Fe_3O_4 Nanofluids

5. Conclusion

This study investigated the density variations of single, bi-hybrid, and ternary-hybrid nanofluids through experimental measurements and machine learning models. The findings revealed that single Al_2O_3 nanofluids exhibited a linear decrease in density with increasing temperature and an increase with higher nanoparticle volume fractions. DIW-based nanofluids demonstrated greater temperature stability, while EG-based systems exhibited higher densities. The introduction of MWCNT nanoparticles in bi-hybrid nanofluids further enhanced density, with EG-based systems achieving the highest values, followed by DIW-EG and DIW-based formulations. The addition of Fe_3O_4 nanoparticles in ternary-hybrid nanofluids resulted in a further increase in density, particularly in EG-based systems and at higher nanoparticle concentrations.

Machine learning models effectively predicted nanofluid density using temperature, nanoparticle volume fraction, and ethylene glycol percentage as key input variables. Linear regression models demonstrated high predictive accuracy, while feature importance analysis identified nanoparticle volume fraction and ethylene glycol content as the most influential factors. Among classification models, Random Forest and logistic regression provided the most robust performance, highlighting their suitability for nanofluid density prediction.

These findings underscore the significant impact of nanoparticle hybridization on nanofluid density and its implications for advanced thermal management systems. The integration of machine learning models offers a reliable approach for predicting density variations, facilitating optimized nanofluid design for renewable energy applications such as solar thermal and geothermal systems. Future research should explore the scalability of hybrid nanofluids and refine predictive models to enhance their practical application in energy and industrial systems.

Nomenclature

T	Temperature
t	Thickness
Greek Characters	
φ	Volume fraction
ρ	Density
δ	interfacial thickness
Abbreviations	
Al_2O_3	Alumina oxide
MWCNT	Multi-Walled Carbon Nanotube
SDBS	Sodium DodecylBenzene Sulfonate
SDBS	Sodium Benzene Sulfonate
Fe_3O_4	Iron III Oxide
DIW	De-ionized Water
EG	Ethylene Glycol
MAE	Mean Absolute Error
vol%	Volume percentage
Subscripts and superscripts	
i	initial
f	final
n	number of item
p	particle
pp	primary particle
cc	complex cluster
nf	nanofluid
p	particle

Acknowledgments

The authors sincerely appreciate Ms. Charity from the Microscopy Department, University of Pretoria, for her invaluable support in conducting the morphology imaging analyses. Additionally, we extend our gratitude to the dedicated technical staff, Mr. Chris and Mr. Donald, from the Nanofluid Research Laboratory, University of Pretoria, for their essential contributions and assistance in completing this research.

CRediT Author Contributions

Emmanuel O. Atofarati: Involved in data collection, conducting experiments, validating results, analysing findings, and preparing the initial draft of the manuscript. **Christopher Enweremadu**: Reviewing and revising the manuscript.

Declaration of Competing Interests

The authors confirm that there are no financial conflicts or personal relationships that could affect the integrity of the work presented in this paper.

Declaration of generative AI and AI-assisted Technologies

During the preparation of this work the author(s) used ChatGPT for language editing. After using this tool/service, the author(s) reviewed and edited the content as needed and take(s) full responsibility for the content of the publication.

Data Availability

The data will be available upon request from the corresponding author.

References

[1] Y Hwang, JK Lee, JK Lee, YM Jeong, S Cheong, YC Ahn, SH Kim, "Production and dispersion stability of nanoparticles in nanofluids," *Powder Technol.*, vol. 186, no. 2, pp. 145–153, Aug. 2008, doi: 10.1016/J.POWTEC.2007.11.020.

[2] S. O. Obayopo, E. O. Atofarati, M. Oyekunle, A. Akintayo, and O. Olayemi, "CFD Analysis of the Thermal Enhancement of PEM Fuel Cell Cooling Channel using Different Cross Sectional Geometry," in *The 13th International Multi-Conference on ICT Applications*, 2019, pp. 129–135, Accessed: Jul. 24, 2024. [Online]. Available:

https://www.researchgate.net/publication/381232281_CFD_ANALYSIS_OF_THE_THERMAL_ENHANCEMENT_OF_PEM_FUEL_CELL_COOLING_CHANNEL_USING_DIFFERENT_CROSS_SECTIONAL_GEOMETRY.
[3] I. U. Ibrahim, M. Sharifpur, J. P. Meyer, and S. M. S. Murshed, "Experimental investigations of effects of nanoparticle size on force convective heat transfer characteristics of Al2O3 - MWCNT hybrid nanofluids in transitional flow regime," *Int. J. Heat Mass Transf.*, vol. 228, p. 125597, Aug. 2024, doi: 10.1016/J.IJHEATMASSTRANSFER.2024.125597.
[4] V. O. Adogbeji, M. Sharifpur, and J. P. Meyer, "Experimental investigation into heat transfer and flow characteristics of magnetic hybrid nanofluid (Fe3O4/TiO2) in turbulent region," *Appl. Therm. Eng.*, vol. 258, p. 124630, Jan. 2025, doi: 10.1016/J.APPLTHERMALENG.2024.124630.
[5] P Sharma, Z Said, A Kumar, S Nizetic, A Pandey, AT Hoang, Z Huang, A Afzal, C Li, AT Le, XP Nguyen, VD Tran, "Recent Advances in Machine Learning Research for Nanofluid-Based Heat Transfer in Renewable Energy System," *Energy and Fuels*, vol. 36, no. 13, pp. 6626–6658, Jul. 2022, doi: 10.1021/ACS.ENERGYFUELS.2C01006/ASSET/IMAGES/MEDIUM/EF2C01006_0008.GIF.
[6] K. Khanafer and K. Vafai, "A review on the applications of nanofluids in solar energy field," *Renew. Energy*, vol. 123, pp. 398–406, Aug. 2018, doi: 10.1016/J.RENENE.2018.01.097.
[7] K Elsaid, MA Abdelkareem, HM Maghrabie, ET Sayed, T Wilberforce, A Baroutaji, AG Olabi, "Thermophysical properties of graphene-based nanofluids," *Int. J. Thermofluids*, vol. 10, p. 100073, May 2021, doi: 10.1016/J.IJFT.2021.100073.
[8] R. S. Vajjha and D. K. Das, "A review and analysis on influence of temperature and concentration of nanofluids on thermophysical properties, heat transfer and pumping power," *Int. J. Heat Mass Transf.*, vol. 55, no. 15–16, pp. 4063–4078, Jul. 2012, doi: 10.1016/J.IJHEATMASSTRANSFER.2012.03.048.
[9] V. O. Adogbeji, E. O. Atofarati, M. Sharifpur, and J. P. Meyer, "Magnetohydrodynamics of nanofluid internal forced convection: A review and outlook for practical applications," *Results Phys.*, vol. 68, p. 108082, Jan. 2025, doi: 10.1016/J.RINP.2024.108082.
[10] N. Wilken, M. Sharifpur, E. O. Atofarati, and J. P. Meyer, "Experimental study on transient and steady-state impinging jet cooling condition with TiO2-Water nanofluids," *Case Stud. Therm. Eng.*, vol. 57, p. 104301, May 2024, doi: 10.1016/J.CSITE.2024.104301.
[11] D. Chavan and A. Pise, "Experimental Investigation of Effective Viscosity and Density of Nanofluids," *Mater. Today Proc.*, vol. 16, pp. 504–515, Jan. 2019, doi: 10.1016/J.MATPR.2019.05.122.
[12] H. Karimi and F. Yousefi, "Application of artificial neural network–genetic algorithm (ANN–GA) to correlation of density in nanofluids," *Fluid Phase Equilib.*, vol. 336, pp. 79–83, Dec. 2012, doi: 10.1016/J.FLUID.2012.08.019.
[13] J. P. Meyer, S. A. Adio, M. Sharifpur, and P. N. Nwosu, "The Viscosity of Nanofluids: A Review of the Theoretical, Empirical, and Numerical Models," *http://dx.doi.org/10.1080/01457632.2015.1057447*, vol. 37, no. 5, pp. 387–421, Mar. 2015, doi: 10.1080/01457632.2015.1057447.
[14] E. O. Atofarati, M. Sharifpur, and J. Meyer, "Hydrodynamic effects of hybrid nanofluid jet on the heat transfer augmentation," *Case Stud. Therm. Eng.*, vol. 51, p. 103536, Nov. 2023, doi: 10.1016/J.CSITE.2023.103536.
[15] Q. Z. Xue, "Model for effective thermal conductivity of nanofluids," *Phys. Lett. A*, vol. 307, no. 5–6, pp. 313–317, Feb. 2003, doi: 10.1016/S0375-9601(02)01728-0.
[16] S. Mukherjee, S. Chakrabarty, P. C. Mishra, and P. Chaudhuri, "Stability and sedimentation characteristics of water based Al2O3 and TiO2 nanofluids," *Proc. Inst. Mech. Eng. Part N J. Nanomater. Nanoeng. Nanosyst.*, vol. 238, no. 1–2, pp. 17–30, Mar. 2024, doi: 10.1177/23977914221127735/ASSET/DBDE76C3-BA7C-4B9E-9FC0-8D18338D579B/ASSETS/IMAGES/LARGE/10.1177_23977914221127735-FIG13.JPG.
[17] J. L. T. Chen, A. N. Oumer, and A. A. Azizuddin, "Stability and density analysis of mango bark and mango leaf nanofluids," *IOP Conf. Ser. Mater. Sci. Eng.*, vol. 863, no. 1, p. 012061, May 2020, doi: 10.1088/1757-899X/863/1/012061.
[18] J. Wang, X. Yang, J. J. Klemeš, K. Tian, T. Ma, and B. Sunden, "A review on nanofluid stability: preparation and application," *Renew. Sustain. Energy Rev.*, vol. 188, p. 113854, Dec. 2023, doi: 10.1016/J.RSER.2023.113854.
[19] M. A. Rahman, S. M. M. Hasnain, S. Pandey, A. Tapalova, N. Akylbekov, and R. Zairov, "Review on Nanofluids:

Preparation, Properties, Stability, and Thermal Performance Augmentation in Heat Transfer Applications," *ACS Omega*, Jul. 2024, doi: 10.1021/ACSOMEGA.4C03279/ASSET/IMAGES/LARGE/AO4C03279_0012.JPEG.
[20] KW Baharin, MN Norizan, NA Shah, IJ Shamsudin, IS Mohamad, MA Rosli, MH Husin, N Abdullah, "Assessing material selection and thermophysical considerations for sustainable nanofluids: A comprehensive review," *Nano-Structures & Nano-Objects*, vol. 37, p. 101090, Feb. 2024, doi: 10.1016/J.NANOSO.2024.101090.
[21] L. E. Nielsen, *Predicting the properties of mixtures : mixture rules in science and engineering*. Lincoln: Marcel Dekker Inc, 1978.
[22] B. C. Pak and Y. I. Cho, "HYDRODYNAMIC AND HEAT TRANSFER STUDY OF DISPERSED FLUIDS WITH SUBMICRON METALLIC OXIDE PARTICLES," *Exp. HEAT Transf. An Int. J.*, vol. 11, no. 2, pp. 151–170, 1998, doi: 10.1080/08916159808946559.
[23] M. Sharifpur, S. Yousefi, and J. P. Meyer, "A new model for density of nanofluids including nanolayer," *Int. Commun. Heat Mass Transf.*, vol. 78, pp. 168–174, Nov. 2016, doi: 10.1016/J.ICHEATMASSTRANSFER.2016.09.010.
[24] R. D. Selvakumar and J. Wu, "A comprehensive model for effective density of nanofluids based on particle clustering and interfacial layer formation," *J. Mol. Liq.*, vol. 292, p. 111415, Oct. 2019, doi: 10.1016/J.MOLLIQ.2019.111415.
[25] E Montazer, E Salami, H Yarmand, ZZ Chowdhury, M Dahari, SN Kazi, A Badarudin, "Development of a new density correlation for carbon-based nanofluids using response surface methodology," *J. Therm. Anal. Calorim.*, vol. 132, no. 2, pp. 1399–1407, May 2018, doi: 10.1007/S10973-018-6978-4/FIGURES/7.
[26] D. Yadav, A. Nirala, R. Kumar, and P. Kumar Singh, "Density variation in nanofluids as a function of concentration and temperature," *Mater. Today Proc.*, vol. 46, pp. 6576–6580, Jan. 2021, doi: 10.1016/J.MATPR.2021.04.052.
[27] S. Akilu, A. T. Baheta, and K. V. Sharma, "Characterization and modelling of density, thermal conductivity, and viscosity of TiN–W/EG nanofluids," *J. Therm. Anal. Calorim.*, vol. 140, no. 4, pp. 1999–2010, May 2020, doi: 10.1007/S10973-019-08902-5/FIGURES/9.
[28] S. Nabati Shoghl, J. Jamali, and M. Keshavarz Moraveji, "Electrical conductivity, viscosity, and density of different nanofluids: An experimental study," *Exp. Therm. Fluid Sci.*, vol. 74, pp. 339–346, Jun. 2016, doi: 10.1016/J.EXPTHERMFLUSCI.2016.01.004.
[29] Z. Said, L. S. Sundar, H. Rezk, A. M. Nassef, H. M. Ali, and M. Sheikholeslami, "Optimizing density, dynamic viscosity, thermal conductivity and specific heat of a hybrid nanofluid obtained experimentally via ANFIS-based model and modern optimization," *J. Mol. Liq.*, vol. 321, p. 114287, Jan. 2021, doi: 10.1016/J.MOLLIQ.2020.114287.
[30] Z Said, NK Cakmak, P Sharma, LS Sundar, A Inayat, O Keklikcioglu, C Li, "Synthesis, stability, density, viscosity of ethylene glycol-based ternary hybrid nanofluids: Experimental investigations and model -prediction using modern machine learning techniques," *Powder Technol.*, vol. 400, p. 117190, Mar. 2022, doi: 10.1016/J.POWTEC.2022.117190.
[31] O. Deymi, F. Rezaei, S. Atashrouz, D. Nedeljkovic, A. Mohaddespour, and A. Hemmati-Sarapardeh, "On the evaluation of mono-nanofluids' density using a radial basis function neural network optimized by evolutionary algorithms," *Therm. Sci. Eng. Prog.*, vol. 53, p. 102750, Aug. 2024, doi: 10.1016/J.TSEP.2024.102750.
[32] R. S. Vajjha, D. K. Das, and B. M. Mahagaonkar, "Density Measurement of Different Nanofluids and Their Comparison With Theory," *Pet. Sci. Technol.*, vol. 27, no. 6, pp. 612–624, Apr. 2009, doi: 10.1080/10916460701857714.
[33] M Jamei, M Karbasi, M Mosharaf-Dehkordi, IA Olumegbon, L Abualigah, Z Said, A Asadi, "Estimating the density of hybrid nanofluids for thermal energy application: Application of non-parametric and evolutionary polynomial regression data-intelligent techniques," *Measurement*, vol. 189, p. 110524, Feb. 2022, doi: 10.1016/J.MEASUREMENT.2021.110524.
[34] F. Yousefi and Z. Amoozandeh, "A new model to predict the densities of nanofluids using statistical mechanics and artificial intelligent plus principal component analysis," *Chinese J. Chem. Eng.*, vol. 25, no. 9, pp. 1273–1281, Sep. 2017, doi: 10.1016/J.CJCHE.2016.10.016.
[35] A. Katiyar, A. N. Singh, P. Shukla, and T. Nandi, "Rheological behavior of magnetic nanofluids containing spherical nanoparticles of Fe–Ni," *Powder Technol.*, vol. 224, pp. 86–89, Jul. 2012, doi: 10.1016/J.POWTEC.2012.02.032.
[36] V. O. Adogbeji, M. Sharifpur, and J. P. Meyer, "Experimental investigation of heat transfer, thermal efficiency, pressure

drop, and flow characteristics of Fe3O4-MgO magnetic hybrid nanofluid in transitional flow regimes," *Int. J. Therm. Sci.*, vol. 209, p. 109515, Mar. 2025, doi: 10.1016/J.IJTHERMALSCI.2024.109515.
[37] I. U. Ibrahim, M. Sharifpur, and J. P. Meyer, "Experimental investigations of particle sizes effects on exergy and entropy characteristics of AL2O3 - MWCNT hybrid nanofluid along the transitional flow regime," *Case Stud. Therm. Eng.*, vol. 51, p. 103575, Nov. 2023, doi: 10.1016/J.CSITE.2023.103575.
[38] E. O. Atofarati, M. Sharifpur, and J. P. Meyer, "Pulsating nanofluid-jet impingement cooling and its hydrodynamic effects on heat transfer," *Int. J. Therm. Sci.*, vol. 198, p. 108874, Apr. 2024, doi: 10.1016/J.IJTHERMALSCI.2023.108874.
[39] S. O. Giwa, M. Sharifpur, and J. P. Meyer, "Experimental study of thermo-convection performance of hybrid nanofluids of Al2O3-MWCNT/water in a differentially heated square cavity," *Int. J. Heat Mass Transf.*, vol. 148, p. 119072, Feb. 2020, doi: 10.1016/J.IJHEATMASSTRANSFER.2019.119072.
[40] T. O. Scott, D. R. E. Ewim, and A. C. Eloka-Eboka, "Experimental investigation of natural convection Al2O3-MWCNT/water hybrid nanofluids inside a square cavity," *Exp. Heat Transf.*, vol. 37, no. 3, pp. 294–312, Apr. 2024, doi: 10.1080/08916152.2022.2136284.
[41] I. Umar Ibrahim, M. Sharifpur, and J. P. Meyer, "Mixed Convection Heat Transfer Characteristics of Al2O3 – MWCNT Hybrid Nanofluid under Thermally Developing Flow; Effects of Particles Percentage Weight Composition," *Appl. Therm. Eng.*, vol. 249, p. 123372, Jul. 2024, doi: 10.1016/J.APPLTHERMALENG.2024.123372.
[42] F. N. Jamrus, I. Waini, U. Khan, and A. Ishak, "Effects of magnetohydrodynamics and velocity slip on mixed convective flow of thermally stratified ternary hybrid nanofluid over a stretching/shrinking sheet," *Case Stud. Therm. Eng.*, vol. 55, p. 104161, Mar. 2024, doi: 10.1016/J.CSITE.2024.104161.
[43] D. Dhinesh Kumar and A. Valan Arasu, "A comprehensive review of preparation, characterization, properties and stability of hybrid nanofluids," *Renew. Sustain. Energy Rev.*, vol. 81, pp. 1669–1689, Jan. 2018, doi: 10.1016/J.RSER.2017.05.257.
[44] S. Singh and S. K. Ghosh, "A unique artificial intelligence approach and mathematical model to accurately evaluate viscosity and density of several nanofluids from experimental data," *Colloids Surfaces A Physicochem. Eng. Asp.*, vol. 640, p. 128389, May 2022, doi: 10.1016/J.COLSURFA.2022.128389.
[45] E. O. Atofarati, M. Sharifpur, and Z. Huan, "Nanofluids for heat transfer enhancement: a holistic analysis of research advances, technological progress and regulations for health and safety," *Cogent Eng.*, vol. 11, no. 1, Dec. 2024, doi: 10.1080/23311916.2024.2434623.
[46] E. O. Atofarati, S. Mohsen, and J. P. Meyer, "Parametric influences on nanofluid-jet cooling heat transfer," in *Nanofluids*, vol. 1, Elsevier, 2024, pp. 351–398.
[47] V. O. Adogbeji, M. Sharifpur, and J. P. Meyer, "Experimental investigation of heat transfer, thermal efficiency, pressure drop, and flow characteristics of Fe3O4-MgO magnetic hybrid nanofluid in transitional flow regimes," *Int. J. Therm. Sci.*, vol. 209, p. 109515, Mar. 2025, doi: 10.1016/J.IJTHERMALSCI.2024.109515.
[48] R. J. Moffat, "Describing the uncertainties in experimental results," *Exp. Therm. Fluid Sci.*, vol. 1, no. 1, pp. 3–17, Jan. 1988, doi: 10.1016/0894-1777(88)90043-X.
[49] S. J. Kline, "The Purposes of Uncertainty Analysis," *Trans. ASME*, vol. 107, p. 154, 1985.
[50] E. O. Atofarati, M. Sharifpur, Z. Huan, O. O. Awe, and J. P. Meyer, "Experimental and machine learning study on the influence of nanoparticle size and pulsating flow on heat transfer performance in nanofluid-jet impingement cooling," *Appl. Therm. Eng.*, vol. 258, p. 124631, Jan. 2025, doi: 10.1016/J.APPLTHERMALENG.2024.124631.
[51] O. O. Awe, E. O. Atofarati, M. O. Adeyinka, A. P. Musa, and E. O. Onasanya, "Assessing the factors affecting building construction collapse casualty using machine learning techniques: a case of Lagos, Nigeria," *Int. J. Constr. Manag.*, 2023, doi: 10.1080/15623599.2023.2222966.
[52] V. O. Adogbeji, E. O. Atofarati, M. Sharifpur, and J. P. Meyer, "Experimental Investigation and Machine Learning Modelling of the Effects of Hybridization Mixing Ratio, Nanoparticle Type, and Temperature on the Thermophysical Properties of Fe_3O_4/TiO_2, Fe_3O_4/MgO, and Fe_3O_4/ZnO DI Water Hybrid Ferrofluids," *J. Therm. Anal. Calorim.*, 2025, Accessed: May 15, 2025. [Online]. Available: https://www.editorialmanager.com/jtac/default2.aspx.

[53] J. Çengel, Yunus, A. Ghajar, Afshin, *Heat and Mass Transfer in SI Units: Fundamentals and Applications*, 6th ed. MCGraw Hill, 2020.
[54] D. Bohne, S. Fischer, and E. Obermeier, "Thermal, Conductivity, Density, Viscosity, and Prandtl-Numbers of Ethylene Glycol-Water Mixtures," *Berichte der Bunsengesellschaft für Phys. Chemie*, vol. 88, no. 8, pp. 739–742, Aug. 1984, doi: 10.1002/BBPC.19840880813.